



JOINT INSTITUTE FOR NUCLEAR RESEARCH  
Veksler and Baldin Laboratory of High Energy Physics

## FINAL REPORT ON THE SUMMER STUDENT PROGRAM

Measurement of elliptic and triangular anisotropic  
collective flows at Au+Au collisions  
 $\sqrt{s_{NN}} = 27$  and  $39$  GeV at STAR experiment.

**Supervisor:** Alexey Aparin, JINR

**Student:** Demanov Alexander, Russia  
National Research Nuclear University MEPhI

**Participation Period:** August 01 - September 14

Dubna, 2019

## Abstract

This work is dedicated to study of the elliptic and triangular flow at Au+Au collisions at the energies of BES-I program at STAR experiment at Relativistic Heavy Ion Collider (RHIC). Flow is a measure of azimuthal anisotropy in heavy ion collisions and can be described by the respective coefficients of the azimuthal distribution Fourier decomposition. In this work measurements of the elliptic ( $v_2$ ) and triangular ( $v_3$ ) flow of identified charged hadrons produced in Au+Au collisions at energies  $\sqrt{s_{NN}} = 27$  and 39 GeV are presented. The results obtained for the elliptic flow coincide within the measured uncertainty with the data previously published by the STAR collaboration. In addition new measurements of triangular flow  $v_3$  are conducted for this energies.

# Contents

<b>1</b>	<b>Introduction</b>	<b>4</b>
<b>2</b>	<b>Theory Overview</b>	<b>5</b>
2.1	QGP in heavy ion collisions . . . . .	5
2.2	Azimuthal anisotropy . . . . .	6
2.3	Methods for measuring collective anisotropic flow . . . . .	6
<b>3</b>	<b>STAR Experiment</b>	<b>8</b>
3.1	Time Projection Chamber . . . . .	8
3.2	Time-of-Flight . . . . .	9
<b>4</b>	<b>Experimental data selection</b>	<b>11</b>
4.1	Selection of events and tracks . . . . .	11
4.2	Particle identification . . . . .	13
4.3	Event plane angle corrections . . . . .	14
4.4	Calculation of the event plane resolution . . . . .	15
<b>5</b>	<b>Result of the collective flow measurements</b>	<b>17</b>
5.1	Elliptic flow of charged hadrons . . . . .	17
5.2	Elliptic flow of identified particles . . . . .	19
5.3	Triangular flow of charged hadrons . . . . .	24
5.4	Triangular flow of identified particles . . . . .	27
5.5	$v_2$ and $v_3$ for particle and antiparticle . . . . .	31
<b>6</b>	<b>Conclusion</b>	<b>35</b>
<b>7</b>	<b>Acknowledgments</b>	<b>35</b>

# 1 Introduction

The study of relativistic heavy ions collisions is an interesting and challenging task of modern particle physics.

In 2000, the Relativistic Heavy Ion Collider (RHIC) began to work with heavy ions with energy in the center of mass system that was ten times larger than before. In 2005, at this collider quark-gluon plasma (QGP) was experimentally discovered in the collisions of gold nuclei at energy  $\sqrt{s_{NN}} = 200$  GeV.

In collisions of heavy ions at the RHIC collider, nuclear matter reached the states with extreme temperatures and densities. Under such conditions, a dense hot substance is formed - quark-gluon plasma, in which a phase transition from hadron degrees of freedom to quark-gluon occurs. This produced medium consists of quarks, antiquarks and gluons with colored degrees of freedom being in a state of deconfinement. A similar transition from ordinary nuclear matter to QGM was predicted by lattice calculations in the framework of quantum chromodynamics (QCD) [1,2]. The study of the matter properties in a state of a mixture of quarks and gluons is of considerable interest both in terms of understanding the nature of strong interaction and the origin of elementary particles, and of testing modern theories of the evolution of the early Universe.

In non-central collisions, the nuclei overlapping region has high spatial anisotropy in the plane perpendicular to the direction of the beam. This initial spatial anisotropy passes into anisotropy in momentum space through strong interaction between particles, and can be measured experimentally using notion of the collective flow [3]. The main interest in anisotropic flow is due to the fact it is formed on the early stages of ion collision, thus having high sensitivity to the properties of the system before thermal equilibrium.

The first experiments at RHIC showed that quark-gluon plasma exhibits strong collectivity, demonstrating the properties of rather a liquid that is close to ideal, than to an ideal gas [4,5]. The collective properties of the system can be studied using transverse momentum distributions ( $p_T$ ) and measurements of azimuthal anisotropy in particle distributions. The values of azimuthal anisotropic flow can be determined using the coefficients in the expansion in the Fourier decomposition of the particles azimuthal distribution.

The purpose of this work is to measure elliptic and triangular collective flow for identified charged hadrons in collisions of gold nuclei at energies of  $\sqrt{s_{NN}} = 27, 39$  GeV. For this measurements, we used data from the BES-I (Beam Energy Scan) program of the STAR experiment.

## 2 Theory Overview

### 2.1 QGP in heavy ion collisions

One of the major goals of experimental programs in high-energy nuclear physics is to determine the conditions behind the phase transition between hadronic matter (a state in which quarks and gluons are confined in composite particles, called baryons and mesons) and the QGP (a state of deconfined partonic matter). At high energies, Quantum Chromodynamics (QCD) predicts a phase transition, when hot and dense matter is melting, separating particles into a plasma where colored partons (quarks and gluons) became quasi-free and no longer confined into colorless dublets (mesons) and triplets (barions).

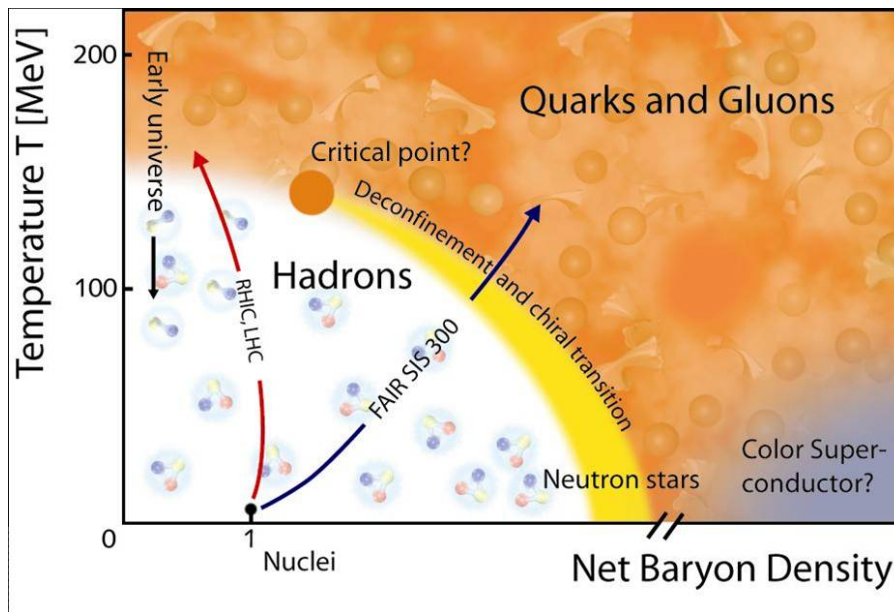


Figure 1: Phase diagram of nuclear matter.

Phase diagram of nuclear matter is shown on Figure 1. Temperature  $T$  is plotted on the ordinate axis, and the density of baryonic matter on the abscissa axis. At low temperatures and nuclear density quarks and gluons are confed in hadrons. Matter is described as hadron gas. At low temperatures with a high density of matter, other hypothetical states of matter arise. In the region of high temperatures and not very high values of the baryon potential, quantum chromodynamics predicts a first-order transition from the hadron gas to the QGP, while at very low baryon densities a cross-over transition is expected.

In 2010, the Relativistic Heavy Ion Collider (RHIC) launched a multi-step experimental program to investigate the phase diagram of strongly interacting nuclear matter. The exploratory phase I of the Beam Energy Scan (BES) [6] program was carried out in 2010, 2011 and 2014 with collisions energy of gold ions ranging from 39 GeV down to 7.7 GeV. This, together with larger data sets

at 62, 130 and 200 GeV, allowed for an initial look into the uncharted territory of QCD phase diagram.

## 2.2 Azimuthal anisotropy

The main purpose of experimental programs for studying collisions of heavy ions at the RHIC relativistic collider is to study the transport properties of strongly interacting quark-gluon plasma (QGP).

An azimuthal anisotropic flow describes a collectivity among particles produced in heavy-ion collision, and it is recognized as one of the key observable which provides information on the early time evolution of the nuclei interaction. Also, this value is sensitive to the transport properties of QGP: the equation of state, velocity of sound, and the value of specific shear viscosity or the ratio of shear viscosity to entropy density.

The hot substance formed in the collision quickly reaches thermodynamic equilibrium through numerous interactions and can be described using hydrodynamic models. In this case, the expansion of the substance happen due to pressure gradients. Due to the initial spatial anisotropy of the nuclei overlapping region, pressure gradients lead to uneven expansion of the substance.

Anisotropic transverse flow is usually quantified by the coefficients (harmonics) in the Fourier decomposition of the azimuthal distribution of particles with respect to the reaction plane [3].

$$E \frac{d^3 N}{d^3 p} = \frac{1}{2\pi} \frac{d^2 N}{p_T dp_T dy} \left( 1 + \sum_{n=1}^{\infty} 2v_n \cos(n(\phi - \Psi)) \right) \quad (1)$$

where  $E$  is particle energy,  $p_T$  - transverse momentum,  $y$  - rapidity,  $\phi$  - azimuthal angle,  $\Psi$  - the angle of the plane of symmetry (reaction plane).

$$v_n = \langle \cos[n(\phi - \Psi)] \rangle \quad (2)$$

coefficients are used for a quantitative characterization of the event anisotropy, and the angle brackets mean an average over all particles in all events. The sine terms are not present because of symmetry with respect to the reaction plane.  $v_1$  is referred to as directed flow,  $v_2$  is referred to as elliptic flow and  $v_3$  as triangular flow.

## 2.3 Methods for measuring collective anisotropic flow

There are different ways to measure collective flow. Each one has different sensitivity to flow fluctuations and non-flow effects. In this paper, we use the Event Plane method [3] which description is presented below.

The reaction plane (RP) is determined by the axis of the beam and the vector of the impact parameter  $\mathbf{b}$  (vector in the transverse plane between the centers

of the nuclei) of the collision. The angle of the reaction plane  $\Psi_{RP}$  cannot be directly measured in the collision, but it can be calculated from the azimuthal distribution of particles in each event.

In the event plane method one estimates the azimuthal angle of the reaction plane from the observed event plane angle determined from the anisotropic flow itself. This is done for each harmonic,  $n$ , of the Fourier decomposition. The event flow vector  $Q_n$  is a 2d vector in the transverse plane:

$$Q_{n,x} = Q_n \cos(n\Psi_n^{EP}) = \sum_i w_i \cos(n\phi_i), \quad (3)$$

$$Q_{n,y} = Q_n \sin(n\Psi_n^{EP}) = \sum_i w_i \sin(n\phi_i), \quad (4)$$

where  $\phi_i$  is the azimuthal angle of the  $i$ -th particle,  $w_i$  is the weight for the  $i$ -th particle. The weight in units of GeV/c was chosen to be linear with  $p_T$  up to 2 GeV/c and then constant at a value of 2 for higher momenta. Event plane angle - azimuthal angle of the  $Q$ -vector, calculated as

$$\Psi_n^{EP} = \frac{1}{n} \tan^{-1} \left( \frac{Q_{n,y}}{Q_{n,x}} \right). \quad (5)$$

But  $\Psi_n^{EP}$  is only an estimate of the angle  $\Psi_{RP}$ , and the desired flow value is:

$$v_n = \langle \cos[n(\phi - \Psi_{RP})] \rangle \quad (6)$$

Using simple transformations, one can get:

$$\begin{aligned} \underbrace{\langle \cos[n(\phi - \Psi_n^{EP})] \rangle}_{v_n^{obs}} &= \langle \cos[n((\phi - \Psi_{RP}) - (\Psi_n^{EP} - \Psi_{RP}))] \rangle = \\ &= \underbrace{\langle \cos[n(\phi - \Psi_{RP})] \rangle}_{v_n} \underbrace{\langle \cos[n(\Psi_n^{EP} - \Psi_{RP})] \rangle}_{Res\{\Psi_n^{EP}\}} \quad (7) \end{aligned}$$

where, after averaging over all events, the terms with sines are equal to zero due to symmetry,  $v_n^{obs}$  is called the observed flow. Correcting  $v_n^{obs}$  to the resolution of the event plane  $Res\{\Psi_n^{EP}\}$  one get the value of the flow  $v_n$ . The resulting formula for determining the  $n$ -th harmonic flow:

$$v_n = \frac{\langle \cos[n(\phi - \Psi_n^{EP})] \rangle}{\langle \cos[n(\Psi_n^{EP} - \Psi_{RP})] \rangle} = \frac{v_n^{obs}}{Res\{\Psi_n^{EP}\}}, \quad (8)$$

The method for calculating the resolution  $Res\{\Psi_n^{EP}\}$  used in this paper is described in Section 4.4.

### 3 STAR Experiment

The Relativistic Heavy Ion Collider (RHIC) is located at Brookhaven National Laboratory (BNL), New York, USA. The main physical tasks of the accelerator are studying the structure of nucleon spin and new state of matter obtained at heavy ion collisions.

STAR (Solenoidal Tracker at RHIC) is a detector complex that specializes in detecting thousands of particles produced by each ion collision. It is used to search for signatures of quark-gluon plasma. STAR consists of several types of detectors, each specializing in detecting certain types of particles or characterizing different aspects of their motion. The scheme of the STAR experiment is shown in Fig.2.

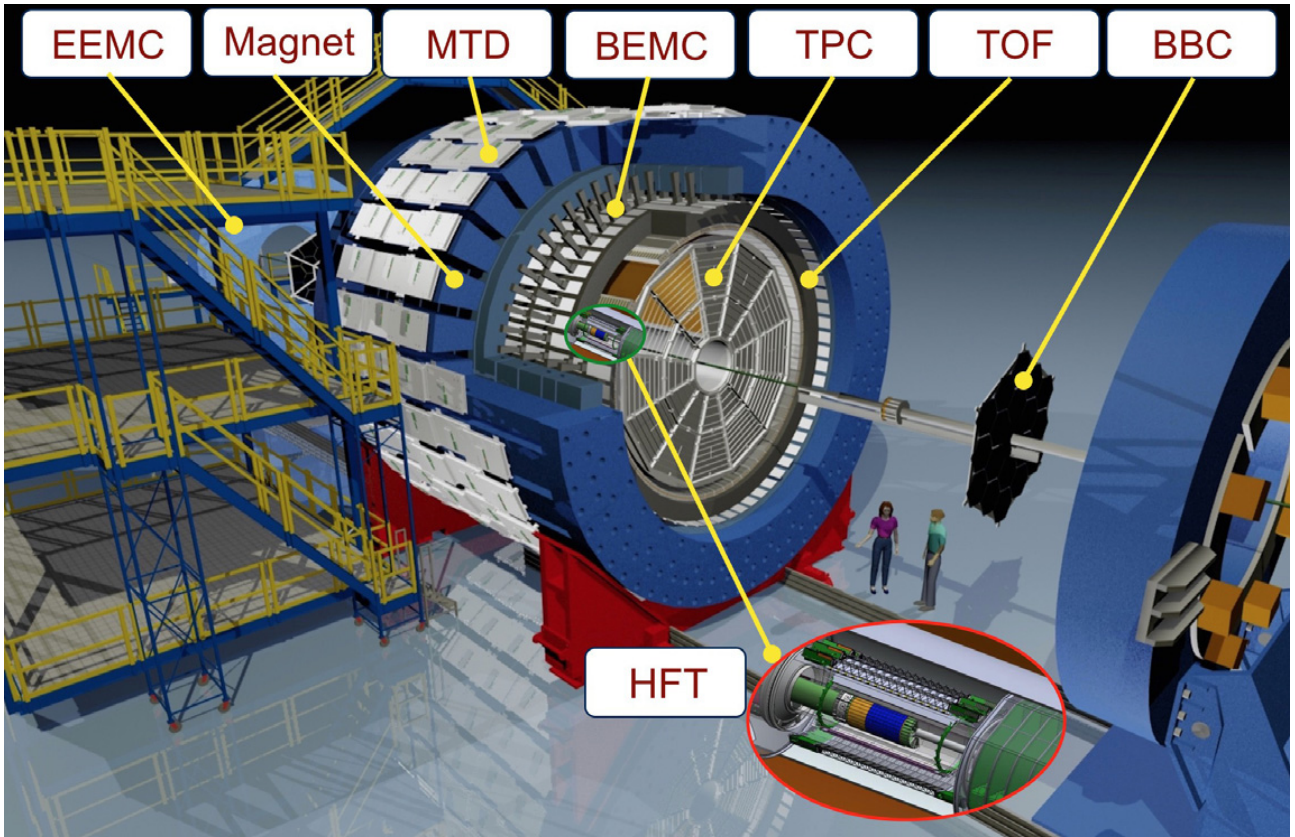


Figure 2: Perspective view of the STAR detector, with a cutaway for viewing inner tracker systems.

In the present work, the following detectors were used to investigate collective flow: Time Projection Chamber (TPC) and Time-of-Flight (TOF) system.

#### 3.1 Time Projection Chamber

The STAR detector uses its TPC as a primary tracking device. The TPC records the tracks of charged particles, measures their momenta, and identifies the particle species by measuring their ionization energy loss ( $dE/dx$ ). Its acceptance

covers  $\pm 1.8$  units of pseudo-rapidity through the full azimuthal angle and over the full range of multiplicities. Charged particles are identified over a momentum range from 100 MeV/c to greater than 1 GeV/c; and momenta are measured over a range of 100 MeV/c to 30 GeV/c. The STAR TPC is shown schematically in Fig. 3. It sits in a large solenoidal magnet that operates at 0.5 T. The TPC is 4.2 m long and 4 m in diameter. It is an empty volume of gas in a well-defined, uniform, electric field of  $\approx 135$  V/cm.

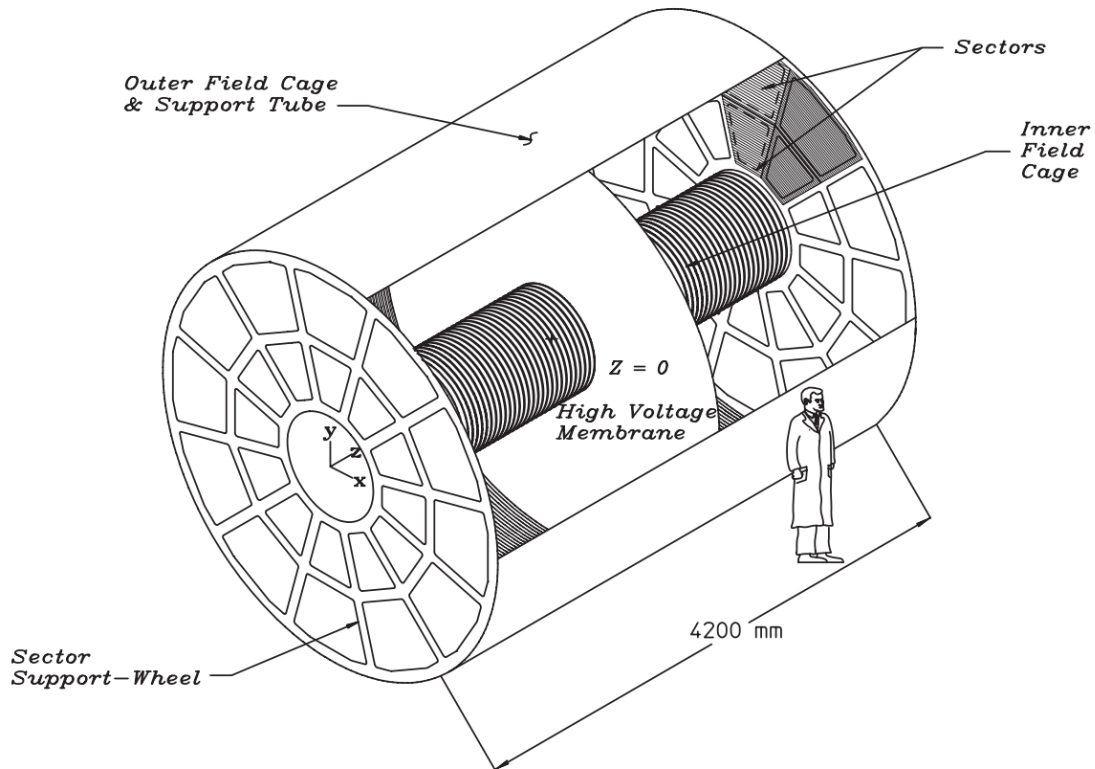


Figure 3: The STAR TPC surrounds a beam–beam interaction region at RHIC.

The paths of primary ionizing particles traversing through the gas volume are reconstructed with high precision from the released secondary electrons which drift to the readout end caps at the ends of the chamber. The uniform electric field which is required to drift the electrons is defined by a thin conductive Central Membrane (CM) at the center of the TPC, concentric field-cage cylinders and the readout end caps. Electric field uniformity is critical since track reconstruction precision is sub-millimeter and electron drift paths are up to 2.1 m.

### 3.2 Time-of-Flight

A segmented time-of-flight system (TOF) is used to increase the possibility of particle registration in the STAR detector complex. It is based on multigap resistive plate chambers (MRPCs). TOF has cylindrical form and placed around

TPC. The system has an intrinsic timing resolution of  $\sim 85$  ps. It covers the full azimuth and a pseudorapidity range of  $-0.9 < \eta < 0.9$ . Time of particle's flight is used for identifying particle species. The particle mass squared,  $m^2$ , can be calculated using the measured TOF and the reconstructed momentum from the TPC.

## 4 Experimental data selection

In this work, we analyzed the data taken by the STAR collaboration in years 2010, 2011 in Au + Au collisions at  $\sqrt{s_{NN}} = 27, 39$  GeV.

### 4.1 Selection of events and tracks

Not all of the detected events are valuable for physics analysis. In order to select only good events a set of cuts was applied to a raw data. Events for analysis were selected based on collision vertex position within 2 cm of the beam axis to reduce contributions from beam-gas and beam-pipe interactions, and the z position of the primary vertices was limited to the values listed in Table1. The 0-80% minimum bias central events for  $v_2$  and  $v_3$  analysis were divided into nine centrality bins: 0-5%, 5-10%, 10-20%, 20-30%, 30-40%, 40-50%, 50-60%, 60-70% and 70-80%.

Table 1: The total number of minimum-bias (MB) events used, and the z-vertex acceptance, for the different energies.

$\sqrt{s_{NN}}$ (GeV)	MB events ( $10^6$ )	z-vertex range (cm)
27	48.6	[-50,50]
39	111.7	[-40,40]

A variety of track quality cuts was used to select only good charged particle tracks reconstructed using information from the TPC. Selection of charged particle tracks criteria:

- primary particle tracks
- pseudo-rapidity range  $|\eta| < 1$
- azimuthal angle range  $0 < \phi < 2\pi$
- We require that the TPC have a number of fit points used for reconstruction of the tracks to be  $>15$  ( $N_{hits}$ )
- the ratio of the number of fit points to maximum possible hits is  $\geq 0,52$  ( $\frac{N_{hits}}{N_{hitsposs}}$ )
- the distance of closest approach (DCA) of the track to the primary vertex  $<2$  cm for event plane reconstruction and DCA  $<1$  cm for flow measurement

An additional transverse momentum cut ( $0.2 < p_T < 2$  GeV/c) is applied to the charged tracks for the TPC event plane reconstruction.

Because data set has been going on for some time, each run has a unique identifier  $RunId = YYDDRRR$ , an eight-digit number. Knowing this number,

one can guarantee identification of the year (2000 + YY - 1), the day of the year (DDD), and the launch number on that day (RRR). Studying the dependence of the average measured characteristics of nuclear collision events on *RunId*, one can see *RunId* at which the average characteristics significantly deviate from the trend. Such *RunId* must be eliminated, since significant deviations can signal failures in the process of data acquisition or accelerator operation. Average values of multiplicity, TOF tray multiplicity, Z-component of event vertex, transverse momentum, energy loss, azimuthal angle, number of hits by RunID were obtained. If average values and errors values went beyond three standard deviations, run was excluded from the analysis. Below are some examples of distributions for each energy 4.

Bad run list  $\sqrt{s_{NN}}=27$  GeV: 12172049, 12172056, 12173009, 12173018, 12173026, 12173053, 12173054, 12173055, 12173056, 12173057, 12173072, 12174077, 12174096, 12174109, 12175007, 12175030, 12175089, 12176046, 12176047, 12176067, 12176069, 12176104, 12178051, 12178093, 12179068, 12179083, 12179084, 12179085, 12179086.

Bad run list for  $\sqrt{s_{NN}}=39$  GeV: 11099102, 11099103, 11099104, 11099106, 11099107, 11099125, 11100004, 11100005, 11100008, 11100010, 11100011, 11100016, 11100020, 11100071, 11101014, 11101104, 11102098, 11103009, 11103047, 11103065, 11105011, 11105029, 11106026, 11106027, 11106028, 11106029, 11106030, 11106040, 11106041, 11107008, 11107046, 11107083, 11108040, 11108053, 11108065, 11108075, 11109092, 11109102, 11109105, 11109104, 11110005, 11110041, 11110042, 11110086.

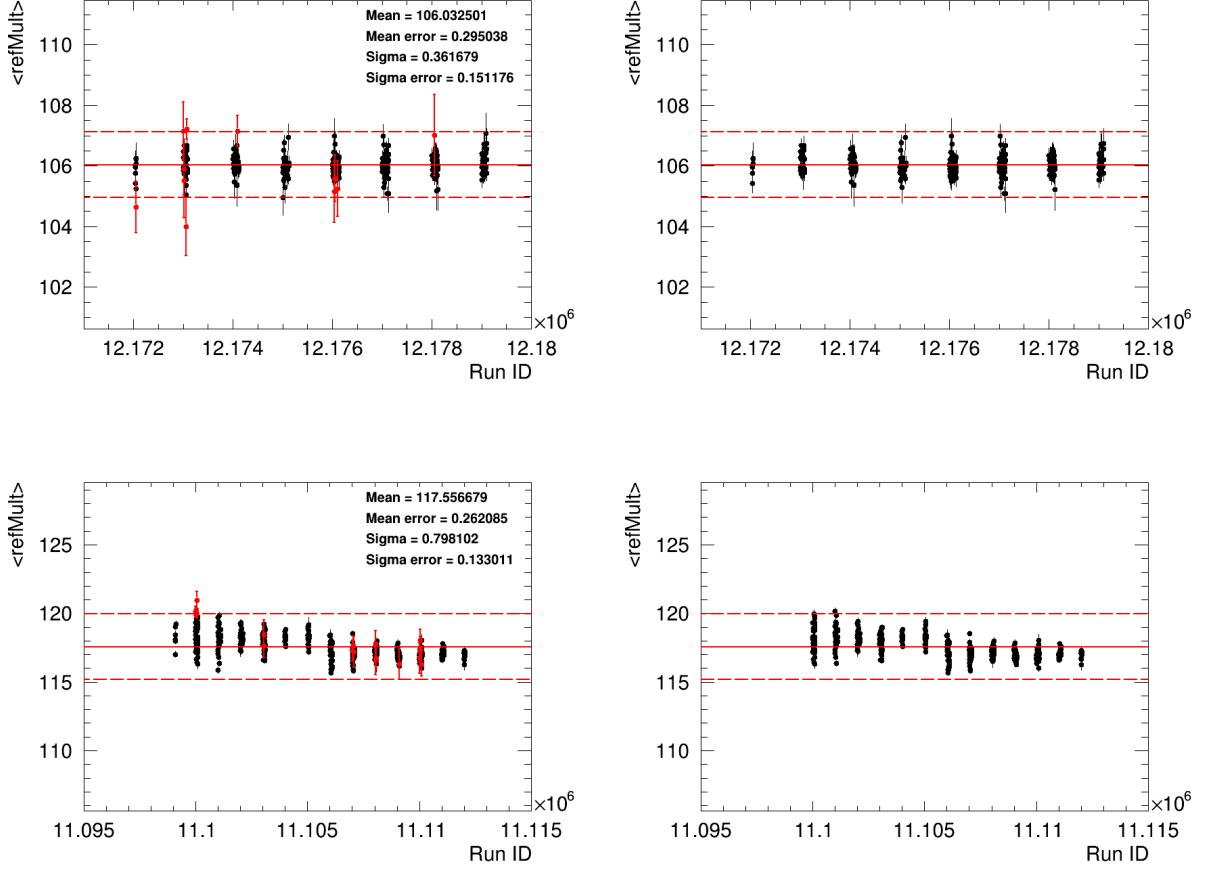


Figure 4: Distribution of multiplicity for Au+Au collisions at  $\sqrt{s_{NN}}=27$  GeV (top pictures) and  $\sqrt{s_{NN}}=39$  GeV (bottom pictures)

## 4.2 Particle identification

Particles can be identified by their mass: the squared mass of the charged hadron is calculated and compared with the table squared value.

To calculate the mass squared, we use the momentum ( $p$ ) reconstructed in the TPC and the flight time  $t_{flight}$ , during which the particle flies through the collision point to the TOF detector:

$$m^2 = p^2 \cdot \left[ \left( \frac{t_{flight}}{L_{track} \cdot c} \right)^2 - 1 \right] \quad (9)$$

where  $p$  is the momentum,  $L_{track}$  is the particle track length. Additionally, a selection was made according to the standard deviation of ionization losses from the theoretical value ( $n\sigma$ ). Particle identification:

Particle	$m^2, (\text{GeV}/c^2)^2, 27 \text{ and } 39 \text{ GeV}$	$ n\sigma , 27 \text{ GeV}$	$ n\sigma , 39 \text{ GeV}$
$\pi^+, \pi^-$	$-0.15 < m^2 < 0.10$	$< 1.5$	$< 3$
$K^+, K^-$	$0.20 < m^2 < 0.32$	$< 1.5$	$< 3$
$p, \bar{p}$	$0.74 < m^2 < 1.20$	$< 1.5$	$< 3$

The picture 5 shows an example of the distribution of the standard deviation of ionization losses from the transverse momentum multiplied by the charge:  $\sqrt{s_{NN}}=27 \text{ GeV}$  on the left,  $\sqrt{s_{NN}}=39 \text{ GeV}$  on the right.

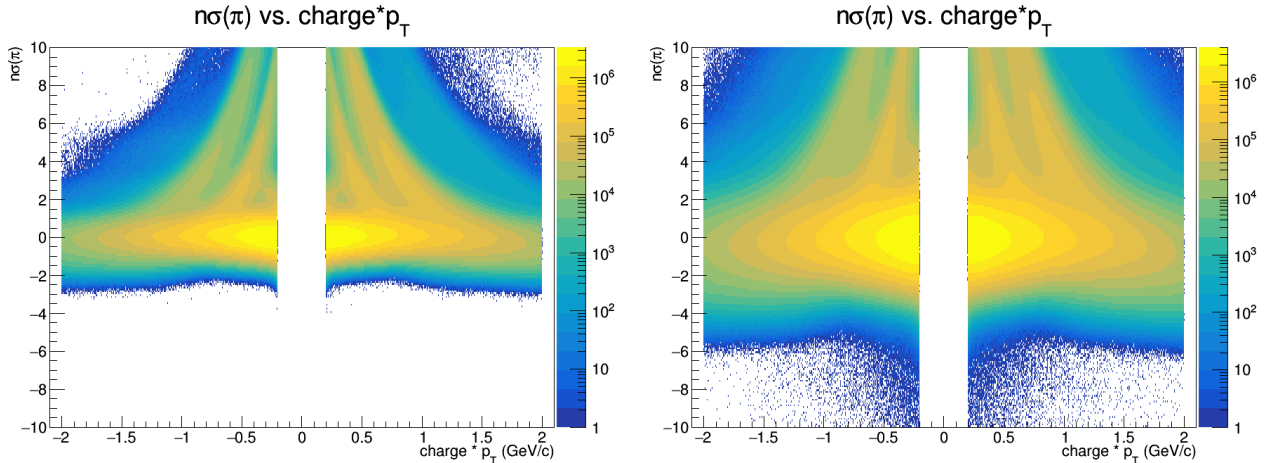


Figure 5: Distribution of the standard deviation of the ionization loss for pions from  $p_T$  times the charge:  $\sqrt{s_{NN}}=27 \text{ GeV}$  on the left,  $\sqrt{s_{NN}}=39 \text{ GeV}$  on the right.

### 4.3 Event plane angle corrections

The 2.3 section shows how to estimate the angle of the event plane (3 - 5), and in this part the correction methods  $\Psi_n^{EP}$  used are presented.

The observed distribution of  $\Psi_n^{EP}$  for all events should be uniform, namely, the average value of  $Q$  of the vector for all events should be 0. But because of the finite acceptance of the detector, the measured value is  $\langle Q_{n,x} \rangle$  and  $\langle Q_{n,y} \rangle$  may shift. To eliminate this effect, the procedure of re-centering the distributions  $Q_{n,x}$   $Q_{n,y}$  (3, 4) in the corresponding intervals by centrality is applied:

$$Q_{n,x(y)}^{rec} = Q_{n,x(y)} - \langle Q_{n,x(y)} \rangle \quad (10)$$

$$\Psi_n^{rec} = \frac{1}{n} \tan^{-1} \left( \frac{Q_{ny}^{rec}}{Q_{nx}^{rec}} \right), \quad (11)$$

The main disadvantage of this method is that it does not remove higher harmonics from the resulting distribution of  $\Psi_n$ . If such harmonics are present then the method requires additional alignment of the event plane distribution. In this case we use flattening procedure (Eq. 12):

$$\Psi_n^{Flat} = \Psi_n^{rec} + \Delta\Psi_n \quad (12)$$

where

$$\Delta\Psi_n = \frac{1}{n} \sum_{i=1}^k \frac{2}{k} [-\langle \sin(kn\Psi_n^{rec}) \rangle \langle \cos(kn\Psi_n^{rec}) \rangle + \langle \cos(kn\Psi_n^{rec}) \rangle \langle \sin(kn\Psi_n^{rec}) \rangle] \quad (13)$$

In equation 13  $i_{max}$  is number of coefficients,  $n$  is harmonic number.

Figure 6 shows distributions of the angle of the event plane  $\Psi_{EP}^{East}$  for centrality 0-5% after successive corrections: before all corrections (left), after re-centering (in the center), after flattening (on the right).

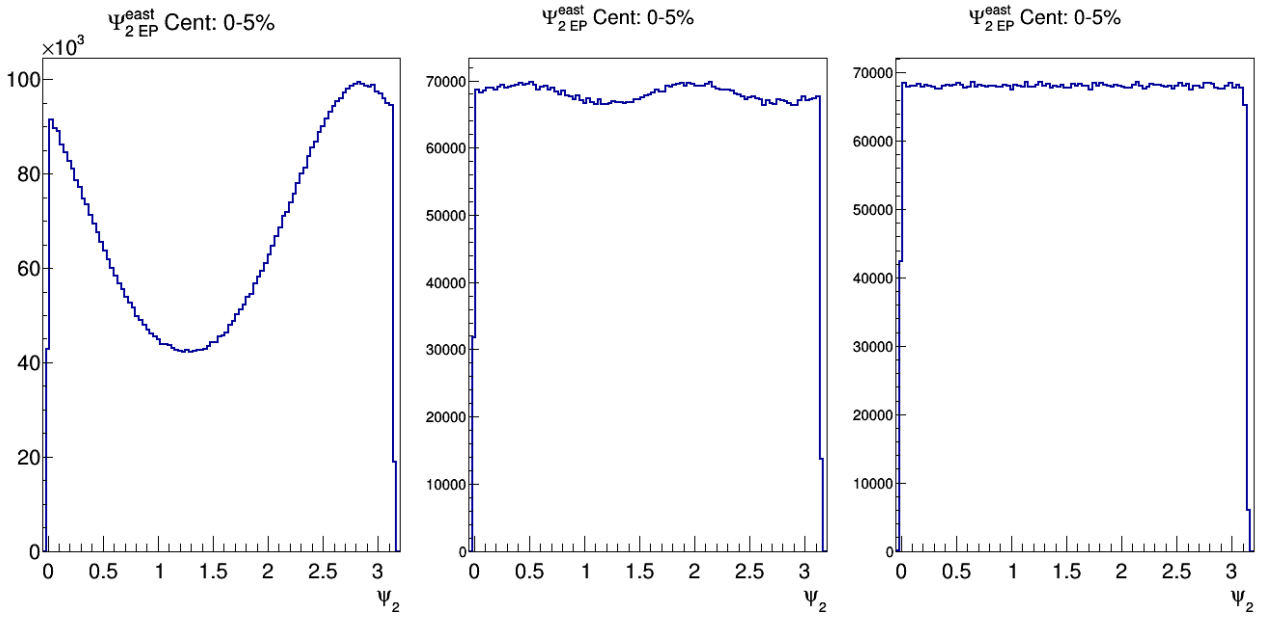


Figure 6: Distributions of the angle of the event plane  $\Psi^{EP}$  after successive corrections: before all corrections (left), after recentering (in the center), after flattening (on the right)

#### 4.4 Calculation of the event plane resolution

To assess the resolution in this work, we are using 2Sub-Event method. The idea of the method is to divide the TPC detector into two segments according to the pseudo-rapidity  $TPC^{East}$  ( $\eta < 0$ ) and  $TPC^{West}$  ( $\eta > 0$ ). To avoid non-flow correlations between the halves, a gap of  $\eta$  is made. The value  $\Delta\eta$  for charged hadrons and identified particles is 0.10. Thus, the resolution of the TPC event plane can be calculated by the formula:

$$Res\{\Psi_n\} = \sqrt{\langle \cos [n(\Psi_{n,\eta_+} - \Psi_{n,\eta_-})] \rangle} \quad (14)$$

where  $\Psi_{n,\eta-}$ ,  $\Psi_{n,\eta+}$  - event plane angles for  $TPC^{East}$  and  $TPC^{West}$  respectively. Then equation 8 can be written:

$$v_n = \frac{\cos(n(\phi_{\pm} - \Psi_{n,\mp}))}{\sqrt{\langle \cos[(n(\Psi_{n,\eta-} - \Psi_{n,\eta+}))] \rangle}} \quad (15)$$

where  $\phi_{\pm}$  - azimuthal angle of east or west track.

Fig.7 shows the dependence of resolution on centrality for  $\sqrt{s_{NN}} = 27$  GeV and  $\sqrt{s_{NN}} = 39$  GeV. The resolution of the event plane decreases with decreasing beam energy due to lower particle multiplicities.

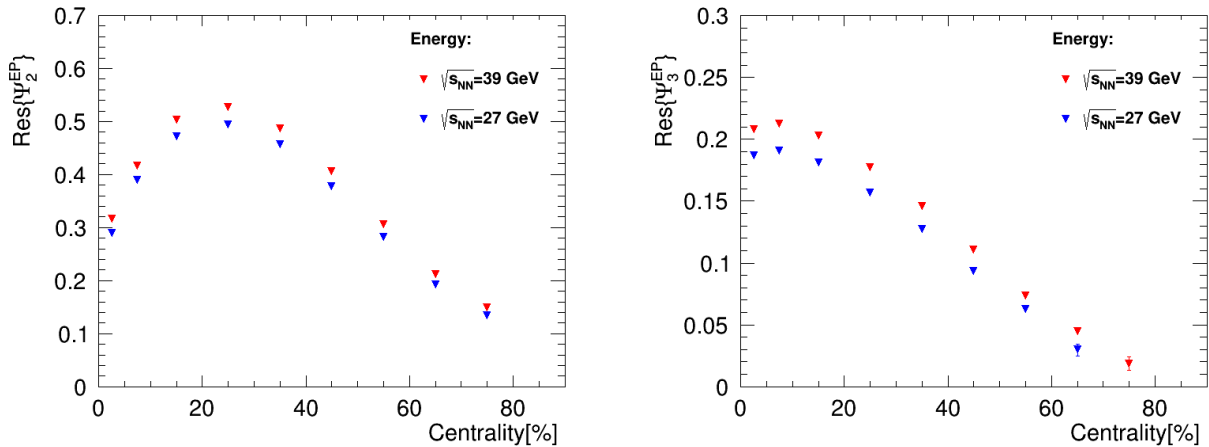


Figure 7: The dependence of the event plane resolution on centrality: left - second harmonics, right - third harmonics

# 5 Result of the collective flow measurements

## 5.1 Elliptic flow of charged hadrons

The values of the elliptic and triangular flows were calculated by Eq. 7. Figures 8 show dependence of the elliptic flow on the transverse momentum for several centrality regions in Au+Au collisions at  $\sqrt{s_{NN}} = 27$  GeV for charged hadrons. Figure 9 show the same for Au+Au collisions at  $\sqrt{s_{NN}} = 39$  GeV. A comparison of the obtained values was made with previous elliptic flow measurements [7], [8]. All values are consistent within the measured error. This leads to a conclude that this method works correctly, and can be used to measure triangular flow.

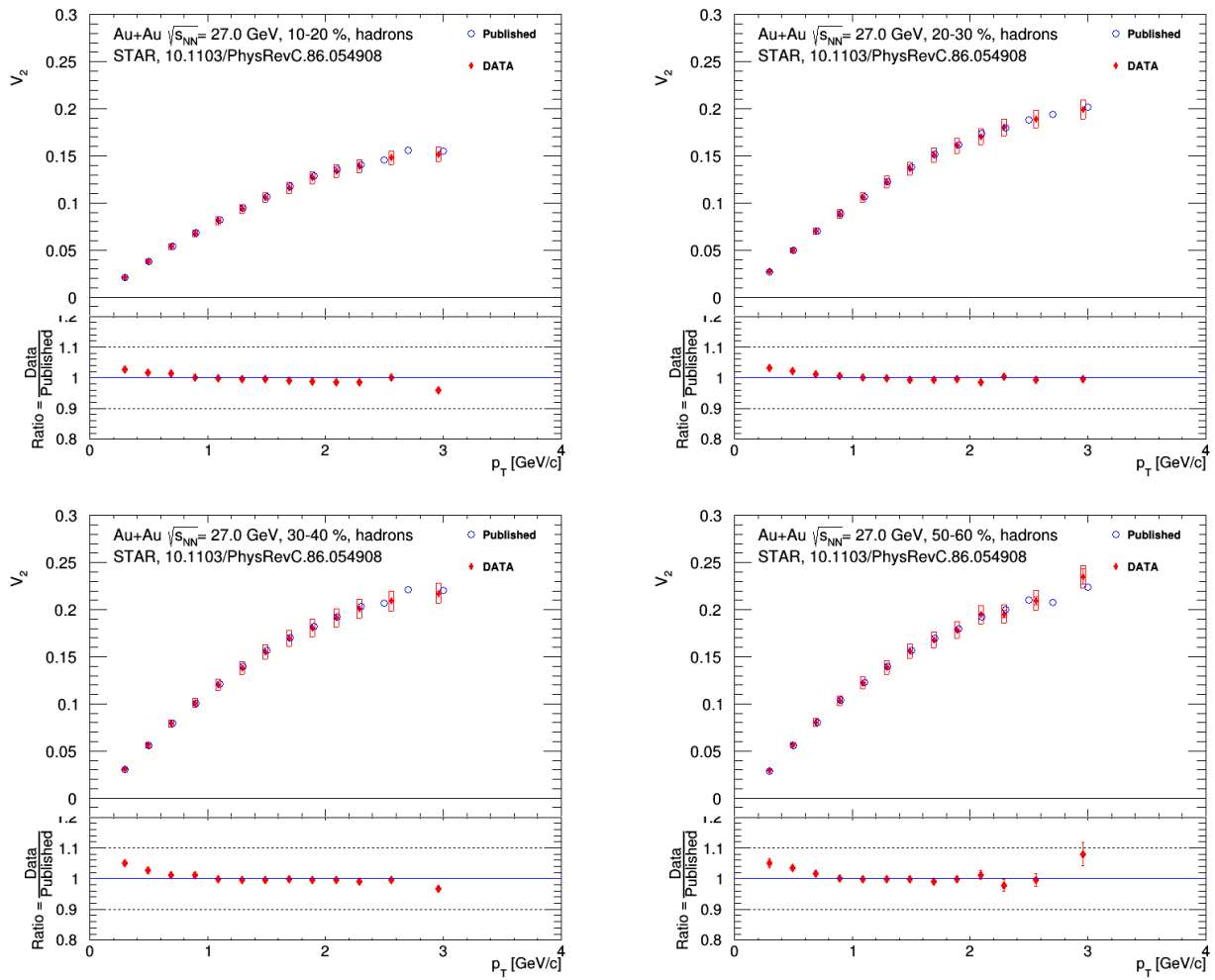


Figure 8: Dependence of the elliptic flow  $v_2$  on the transverse momentum of particles in Au+Au collisions at  $\sqrt{s_{NN}} = 27$  GeV for different centralities. Top pictures: 10-20% on the left and 20-30% on the right, bottom pictures: 30-40% on the left and 50-60% on the right. For each dependence, the ratios of the calculated values of  $v_2$  to published are shown.

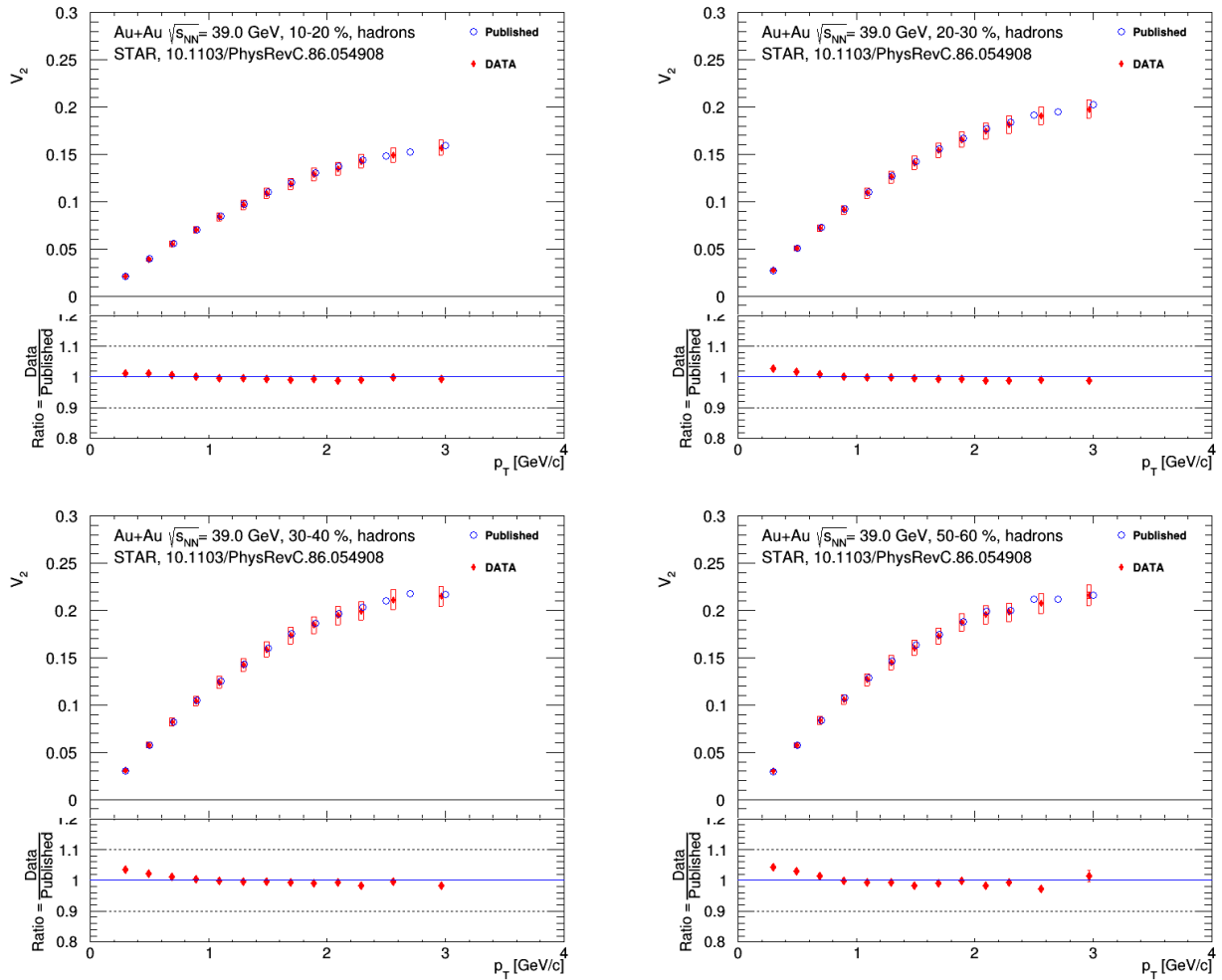


Figure 9: Dependence of the elliptic flow  $v_2$  on the transverse momentum of particles in Au+Au collisions at  $\sqrt{s_{NN}} = 39$  GeV for different centralities. Top pictures: 10-20% on the left and 20-30% on the right, bottom pictures: 30-40% on the left and 50-60% on the right. For each dependence, the ratios of the calculated values of  $v_2$  to published are shown.

Figure 10 shows an elliptic flow as a function of  $p_t$  depending on the centrality of the collision. It is observed that  $v_2$  changes significantly with a change of centrality. Increase of the elliptical flow  $v_2$  up to 50% with centrality is associated with an increase in the ellipticity of the shape of the nuclei overlapping region.

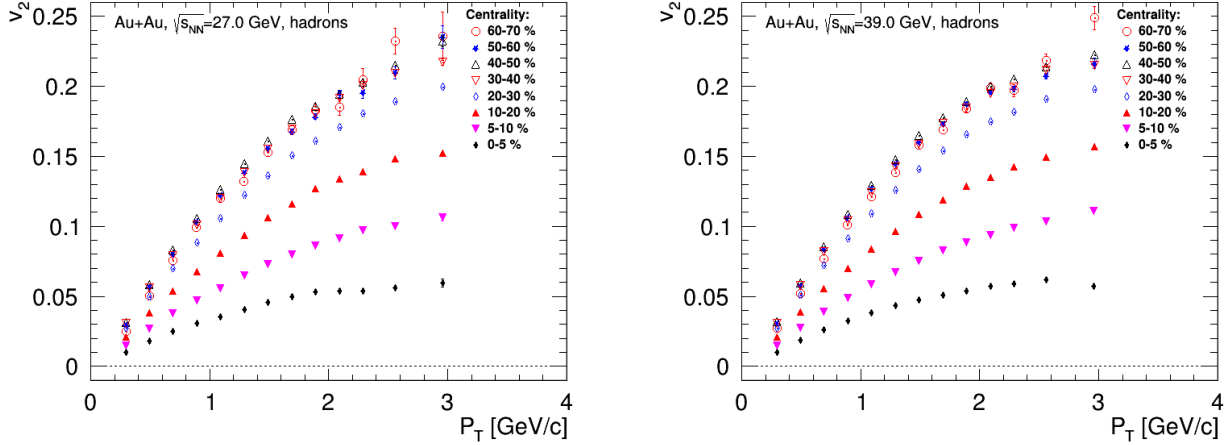


Figure 10: The  $v_2$  as a function of  $p_T$  and centrality collision:  $\sqrt{s_{NN}} = 27$  GeV on the left,  $\sqrt{s_{NN}} = 39$  GeV on the right.

## 5.2 Elliptic flow of identified particles

In order to verify the correctness of the particles identification, the elliptic flow of the identified hadrons was measured (Fig.11) for Au + Au collisions at an energy of  $\sqrt{s_{NN}} = 39$  GeV. A comparison of obtained values was made with previous elliptic flow measurements [8]. All values are consistent within the measured error. this can lead to a conclusion that the used particle identification method works.

Figures 12 and 13 show elliptic flow  $v_2$  for particles and antiparticles as a function of the transverse momentum  $p_T$  for 0%-40% and 30%-60% centrality Au+Au collisions at  $\sqrt{s_{NN}} = 27, 39$  GeV. In the low  $p_T$  region ( $p_T < 1.6$  GeV/c), the  $v_2$  follows mass ordering, where the  $v_2$  of heavier hadrons is lower than that of lighter hadrons. For  $p_T > 1.6$ , a separation of particle flow is observed depending on the number of constituent quarks. This is explained by the quark coalescence mechanism [9], in which the formation of hadrons occurs through the combination of valence quarks. This mechanism predicts the existence of flow scaling  $v_n$  by the number of quarks  $n_q$ . Figures 14 and 15 show scaling of the elliptic flow  $v_2$  particles and antiparticles respectively.

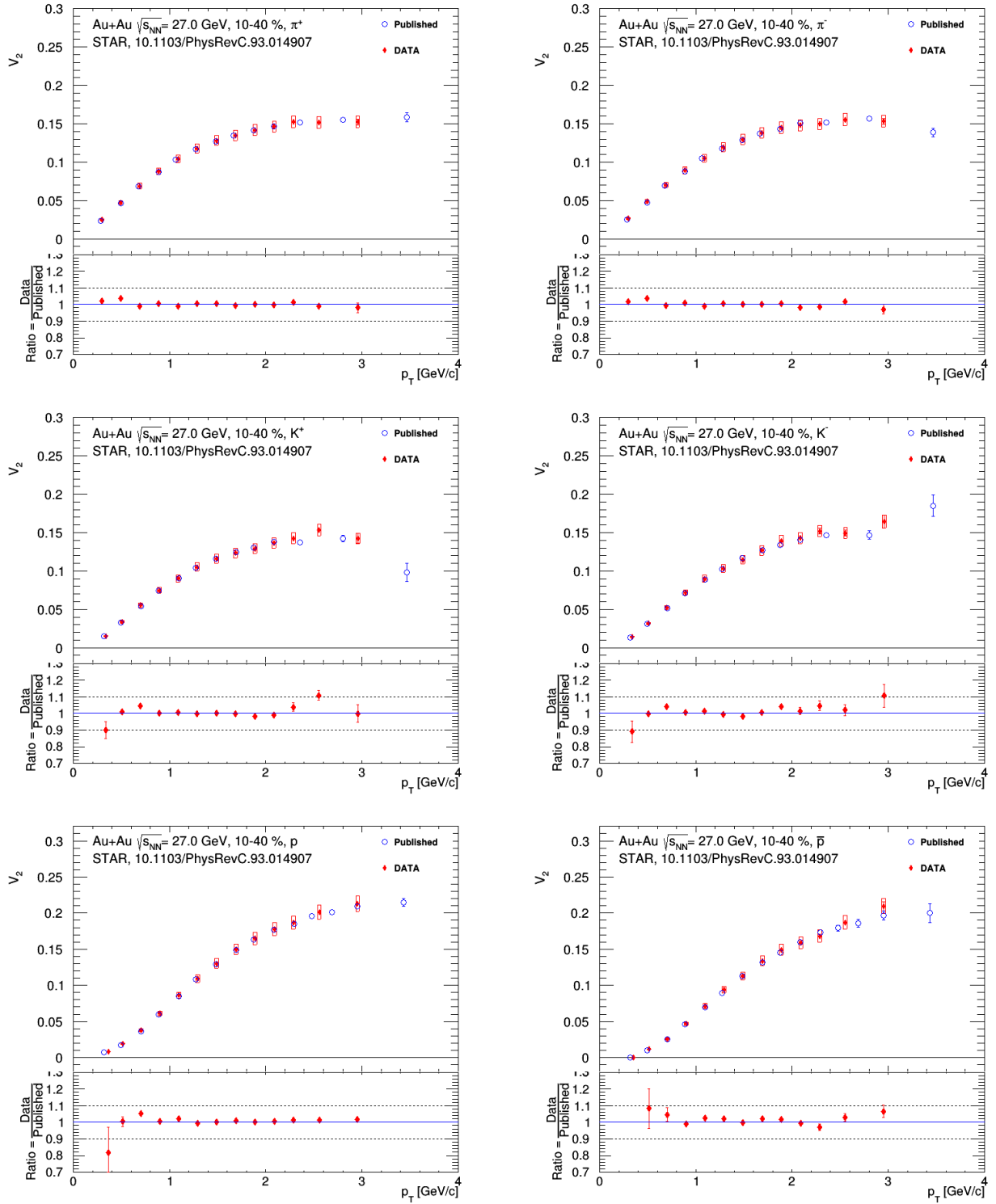


Figure 11: Dependence of the  $v_2$  identified charged hadrons on the transverse momentum of particles in Au+Au collisions at  $\sqrt{s_{NN}} = 39$  GeV for 10-40% centrality: top  $\pi^+$  and  $\pi^-$ , the middle  $K^+$  and  $K^-$ , bottom  $p$  and  $\bar{p}$ .

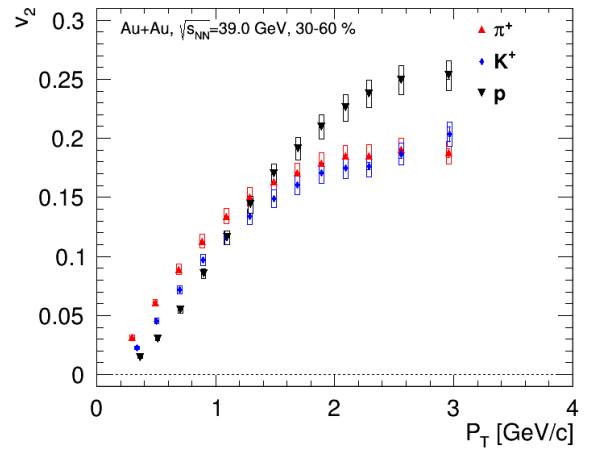
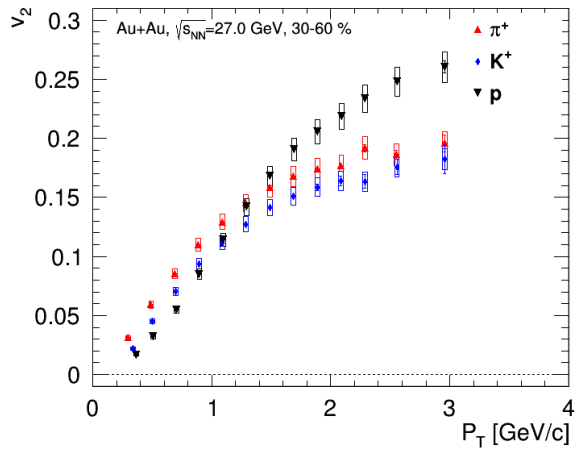
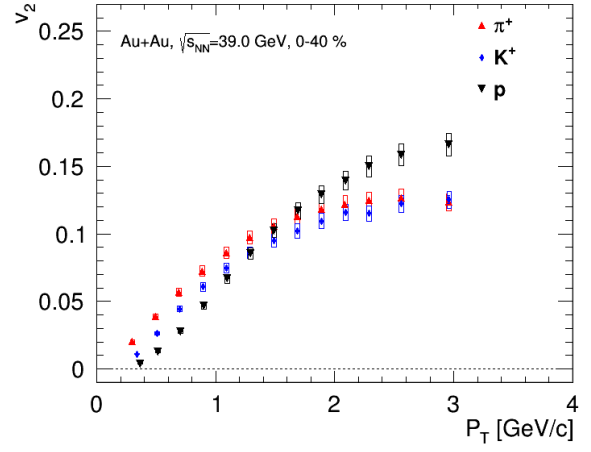
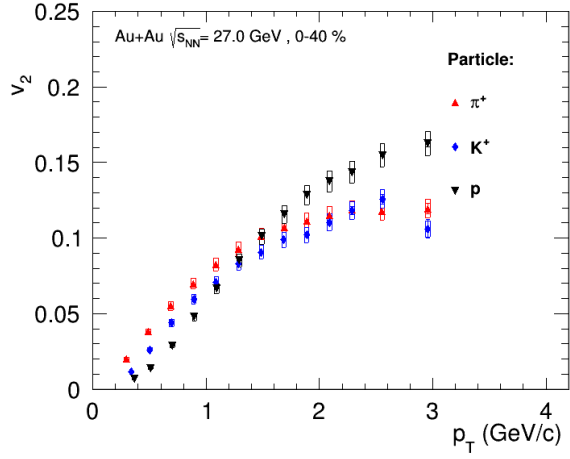


Figure 12: Elliptic flow,  $v_2$ , of particles as a function of the transverse momentum,  $p_T$ , 0%-40%, 30%-60% centrality Au+Au collisions for various particle species and energies: at left - for Au+Au collisions at  $\sqrt{s_{NN}} = 27$ , at right -  $\sqrt{s_{NN}} = 39$  GeV.

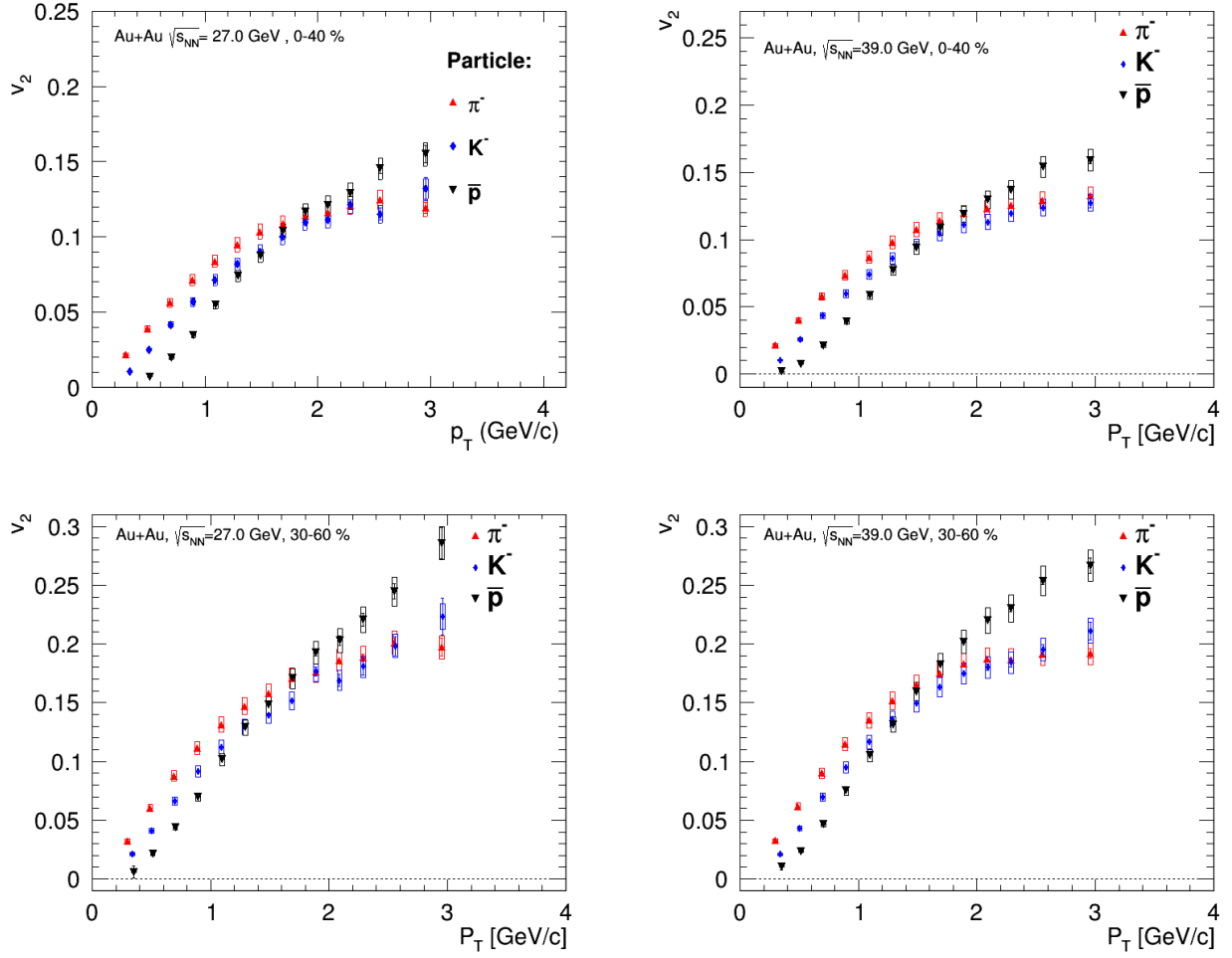


Figure 13: Elliptic flow,  $v_2$ , of antiparticles as a function of the transverse momentum,  $p_T$ , 0%-40%, 30%-60% centrality Au+Au collisions for various particle species and energies: at left - for Au+Au collisions at  $\sqrt{s_{NN}} = 27$ , at right -  $\sqrt{s_{NN}} = 39$  GeV.

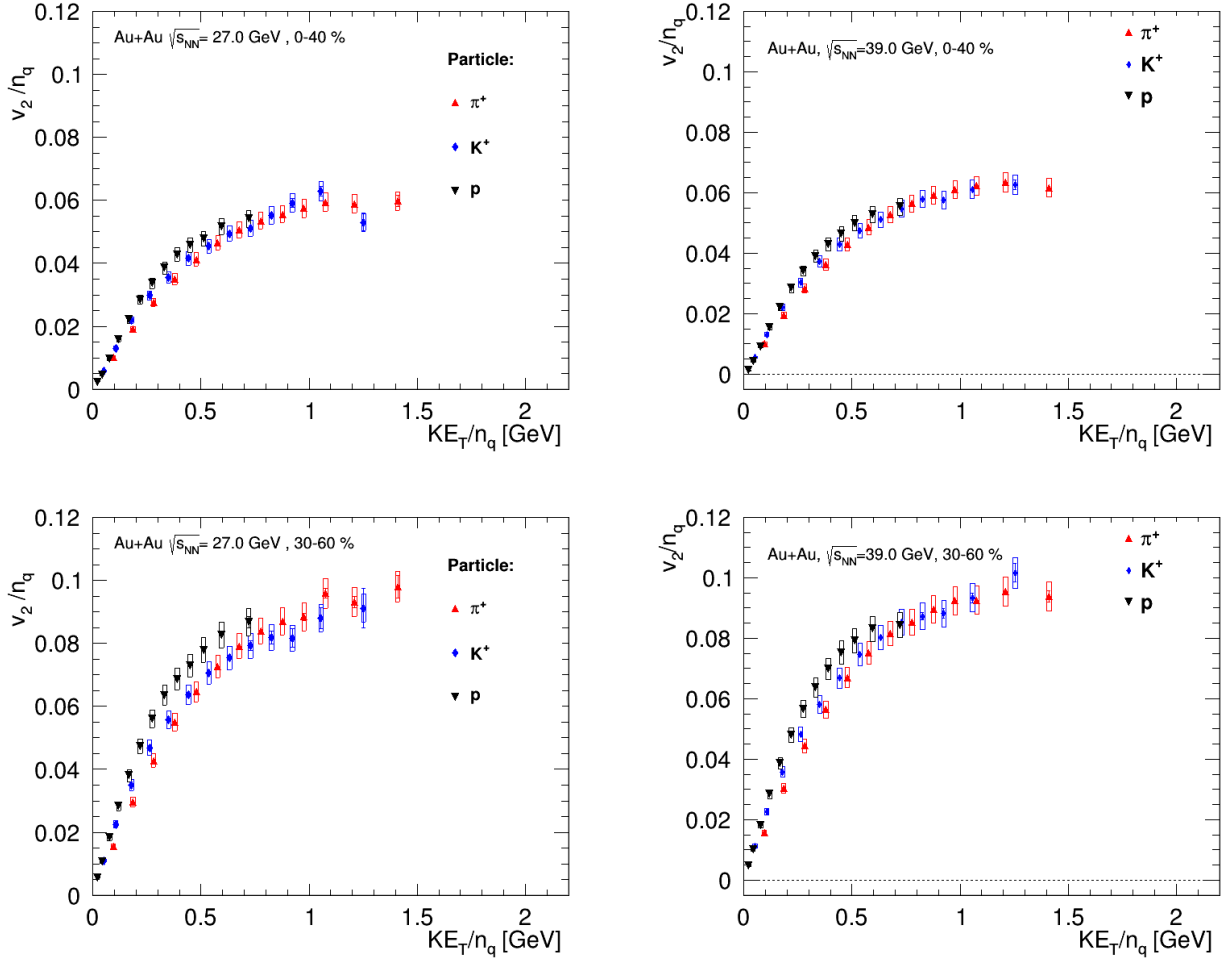


Figure 14: Scaled elliptic flow,  $v_2$ , of particles for 0%-40%, 30%-60% centrality Au+Au collisions for energies: at left - for Au+Au collisions at  $\sqrt{s_{NN}} = 27$ , at right -  $\sqrt{s_{NN}} = 39$  GeV.

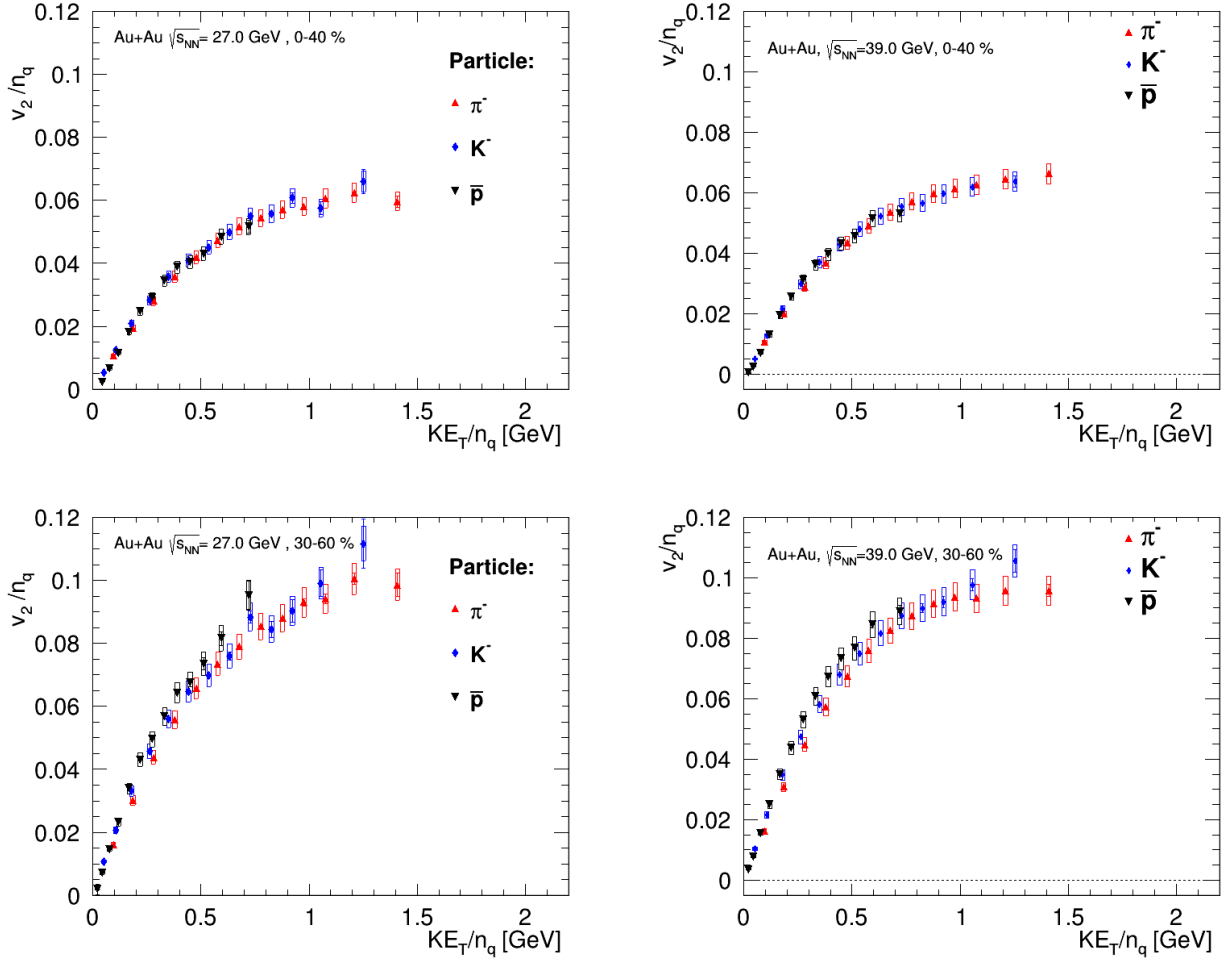


Figure 15: Scaled elliptic flow,  $v_2$ , of antiparticle for 0%-40%, 30%-60% centrality Au+Au collisions for energies: at left - for Au+Au collisions at  $\sqrt{s_{NN}} = 27$ , at right -  $\sqrt{s_{NN}} = 39$  GeV.

### 5.3 Triangular flow of charged hadrons

Figures 16 show dependence of the triangular flow on transverse momentum for several centralities in Au+Au collisions at  $\sqrt{s_{NN}}=27$  GeV for charged hadrons. Figure 17 shows the same for Au+Au collisions at  $\sqrt{s_{NN}}=39$  GeV.

Figure 18 shows an elliptic flow as a function of  $p_T$  depending on the centrality of the collision. It is observed that  $v_3$  almost does not change for different centrality, compared with  $v_2$  (fig.10).

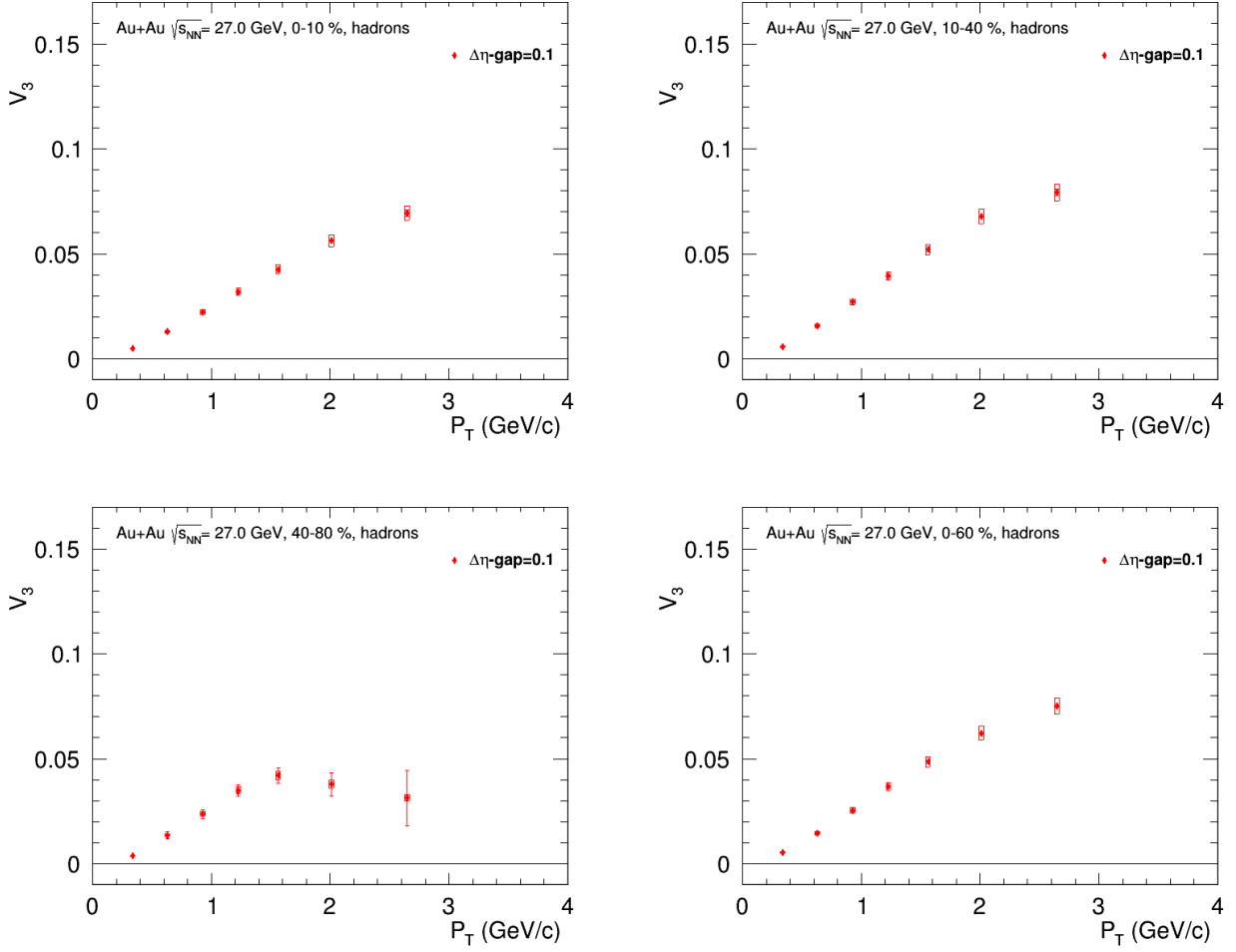


Figure 16: Dependence of the triangular flow  $v_3$  on the transverse momentum of particles in Au+Au collisions at  $\sqrt{s_{NN}} = 27$  GeV for different centralities. Top pictures: 0-10% on the left and 10-40% on the right, bottom pictures: 40-80% on the left and 0-60% on the right. For each dependence, the ratios of the calculated values of  $v_2$  to published are shown.

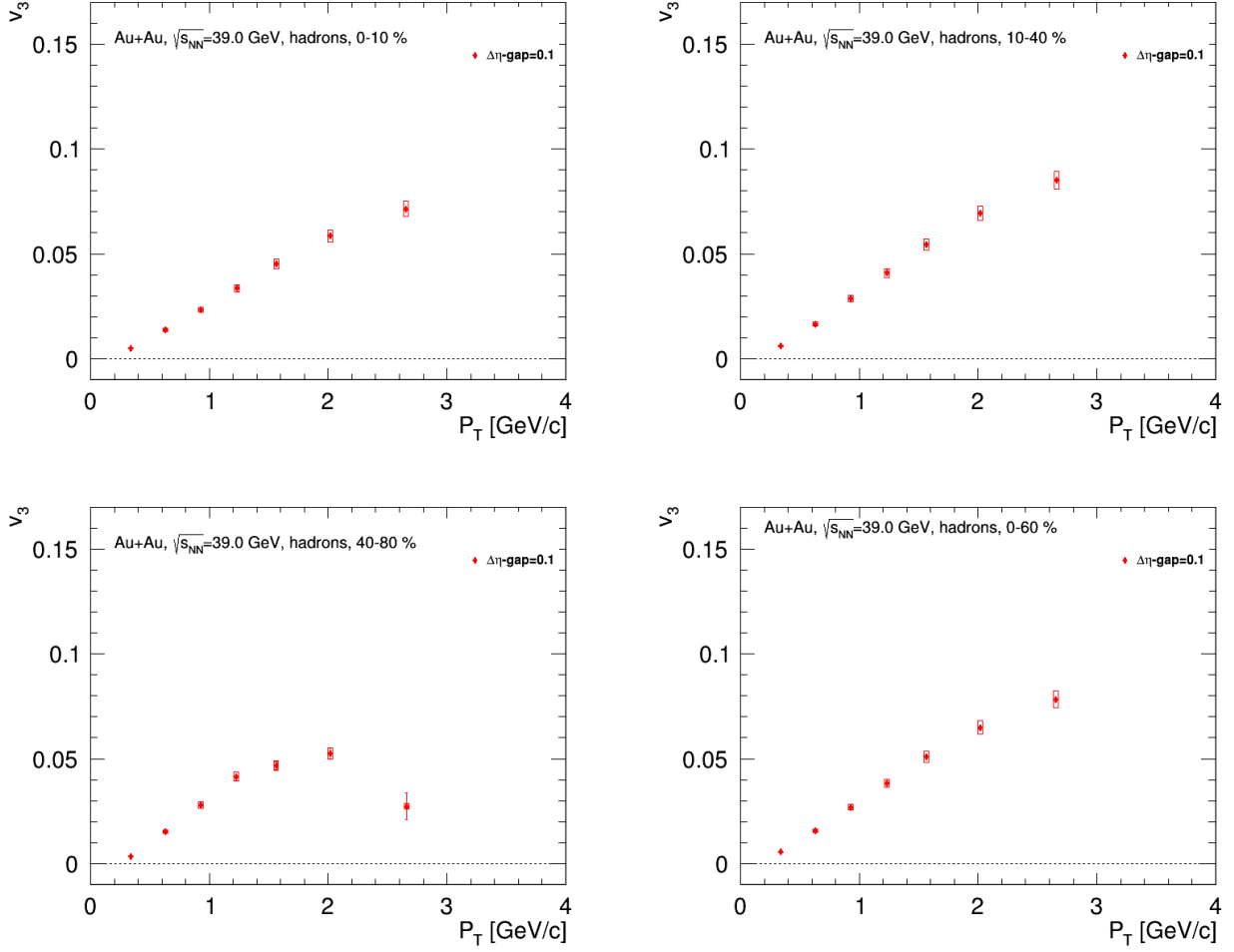


Figure 17: Dependence of the triangular flow  $v_3$  on the transverse momentum of particles in Au+Au collisions at  $\sqrt{s_{NN}} = 39$  GeV for different centralities. Top pictures: 0-10% on the left and 10-40% on the right, bottom pictures: 40-80% on the left and 0-60% on the right. For each dependence, the ratios of the calculated values of  $v_2$  to published are shown.

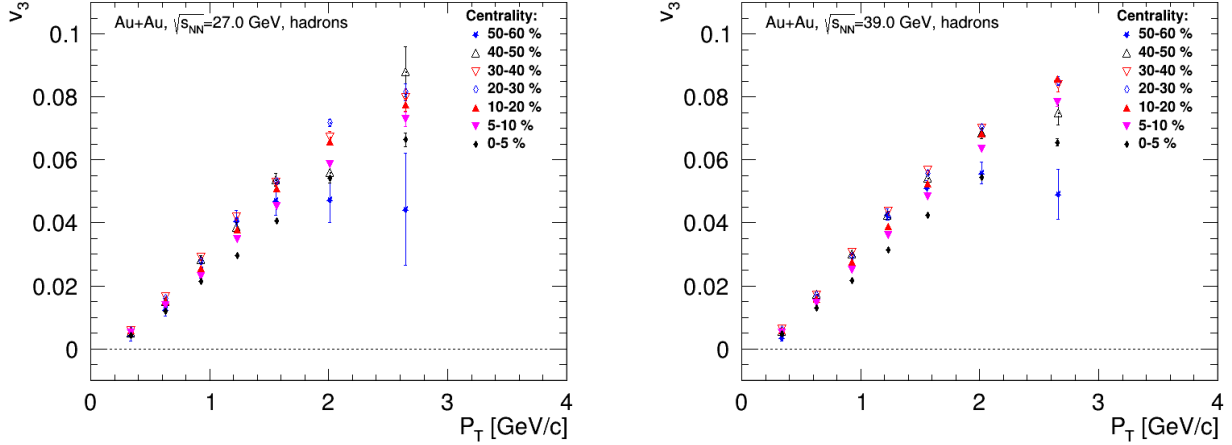


Figure 18: The  $v_3$  as a function of  $p_T$  and centrality of the collision:  $\sqrt{s_{NN}} = 27$  GeV on the left,  $\sqrt{s_{NN}} = 39$  GeV on the right.

## 5.4 Triangular flow of identified particles

Figures 19 and 20 show elliptic flow  $v_2$  for particles and antiparticles as a function of the transverse momentum  $p_T$  for 0%-40% and 30%-60% centrality Au+Au collisions at  $\sqrt{s_{NN}} = 27, 39$  GeV. Observed  $v_3$  follows mass ordering, noticeable dependence on the mass, which disappears in the  $p_T$  region  $> 1.5$ (GeV/c). Figures 14 and 15 show scaled elliptic flow  $v_2$  particles and antiparticles respectively, observed scaling for  $v_3$  is smaller than for  $v_2$  (fig.14,15).

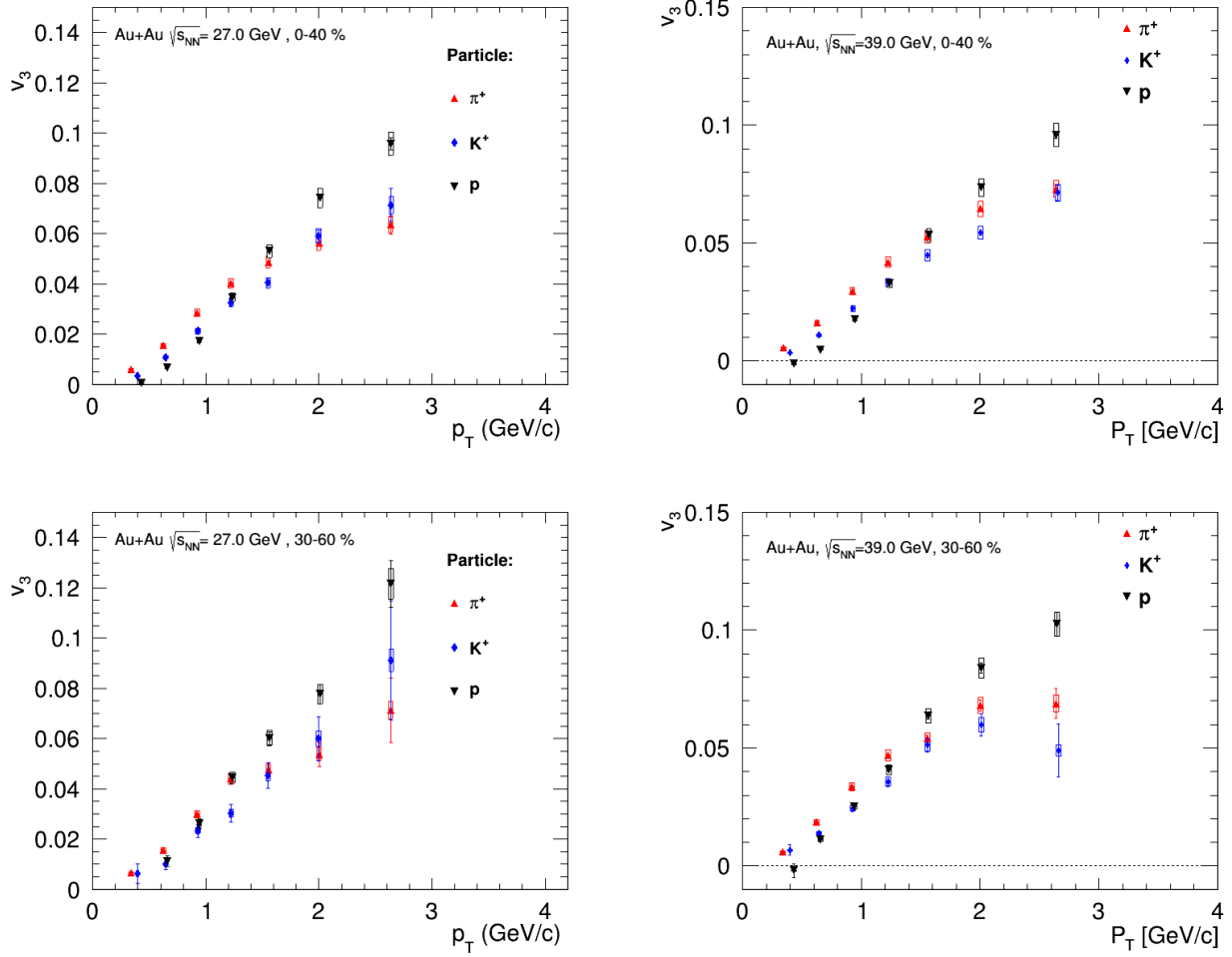


Figure 19: Triangular flow,  $v_3$ , of particles as a function of the transverse momentum,  $p_T$ , 0%-40%, 30%-60% centrality Au+Au collisions for various particle species and energies: on the left - for Au+Au collisions at  $\sqrt{s_{NN}} = 27$ , on the right -  $\sqrt{s_{NN}} = 39$  GeV.

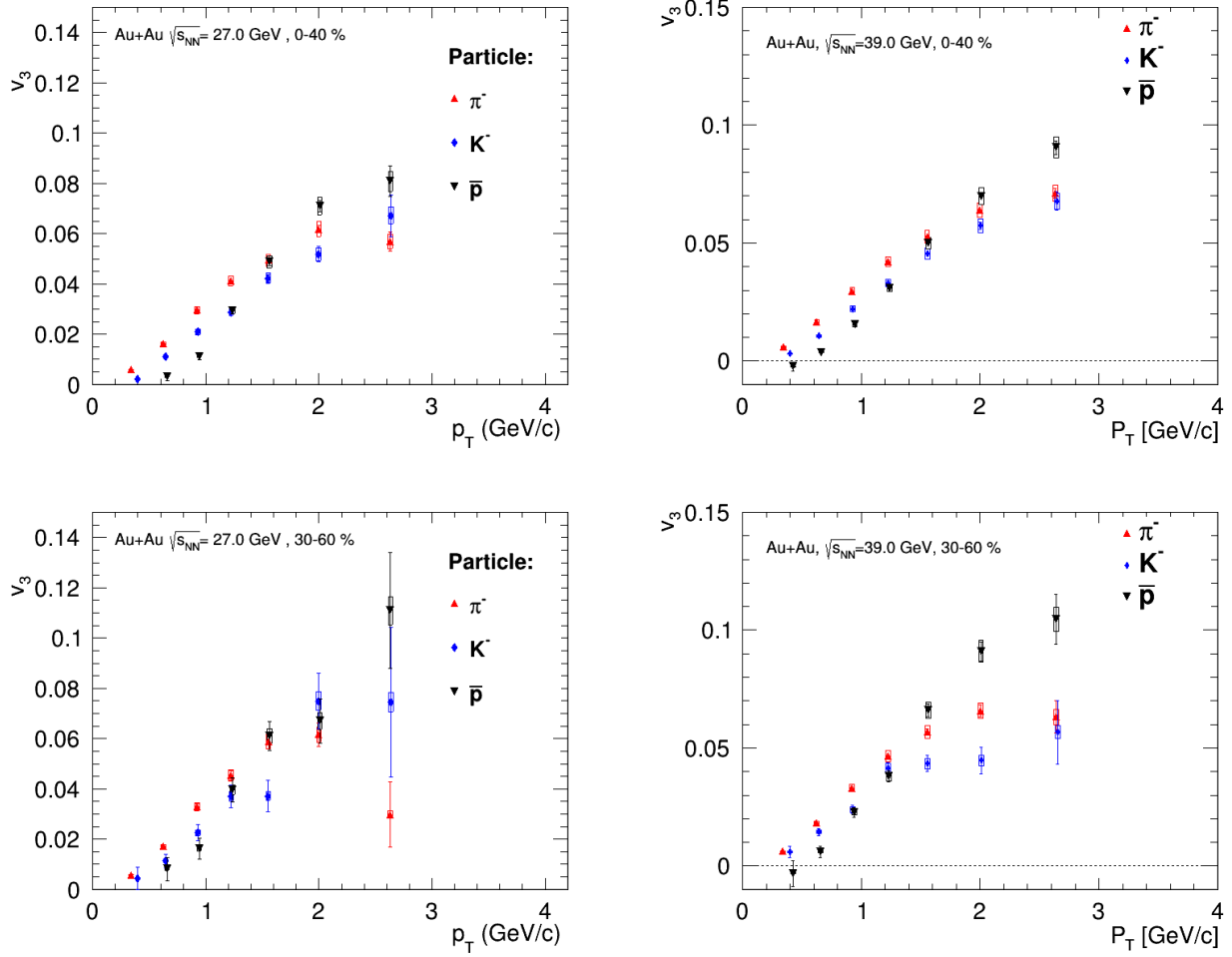


Figure 20: Triangular flow,  $v_3$ , of antiparticles as a function of the transverse momentum,  $p_T$ , 0%-40%, 30%-60% centrality Au+Au collisions for various particle species and energies: on the left - for Au+Au collisions at  $\sqrt{s_{NN}} = 27$ , on the right -  $\sqrt{s_{NN}} = 39$  GeV.

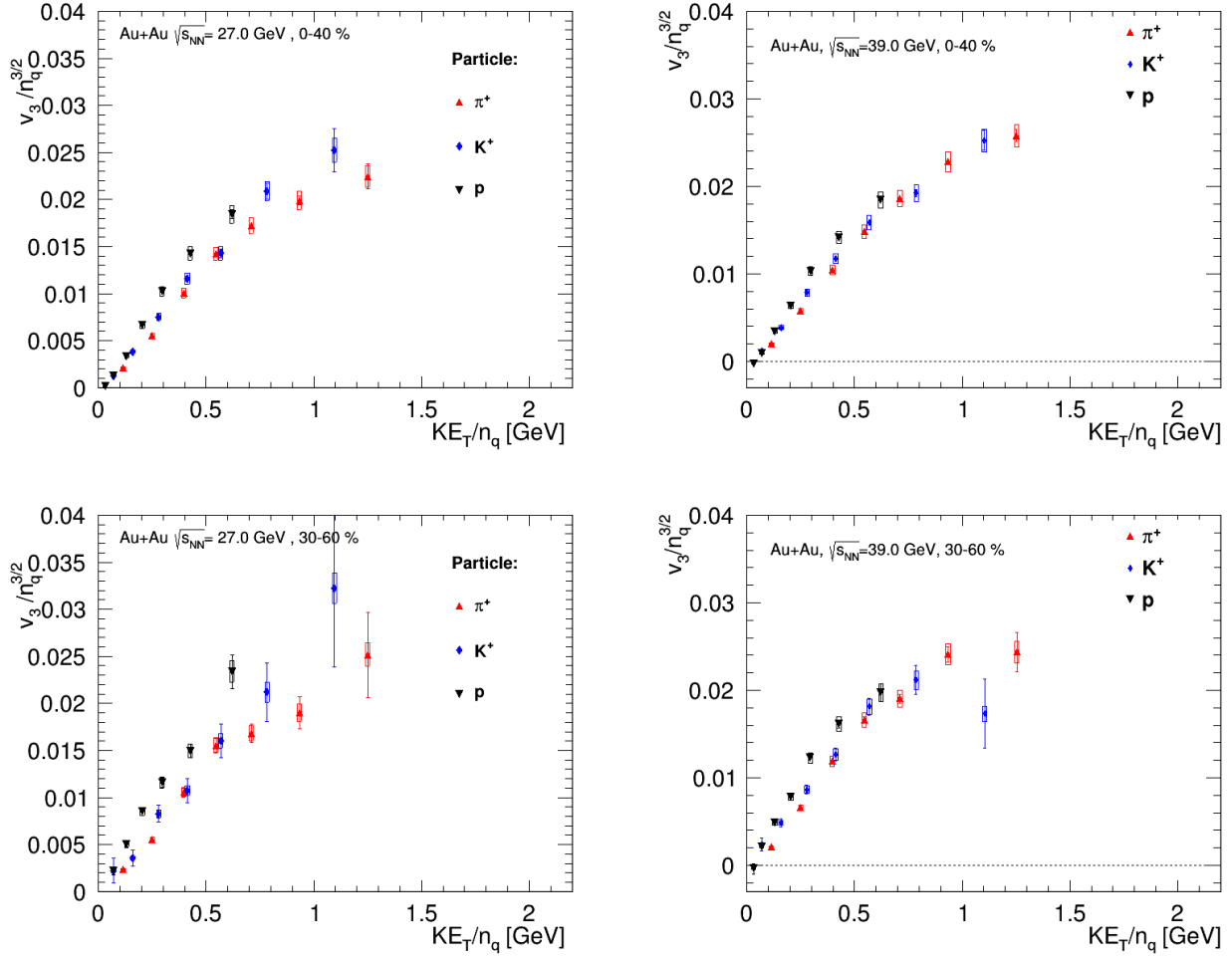


Figure 21: Scaling triangular flow,  $v_3$ , of particles for 0%-40%, 30%-60% centrality Au+Au collisions for energies: on the left - for Au+Au collisions at  $\sqrt{s_{NN}} = 27$ , on the right -  $\sqrt{s_{NN}} = 39$  GeV.

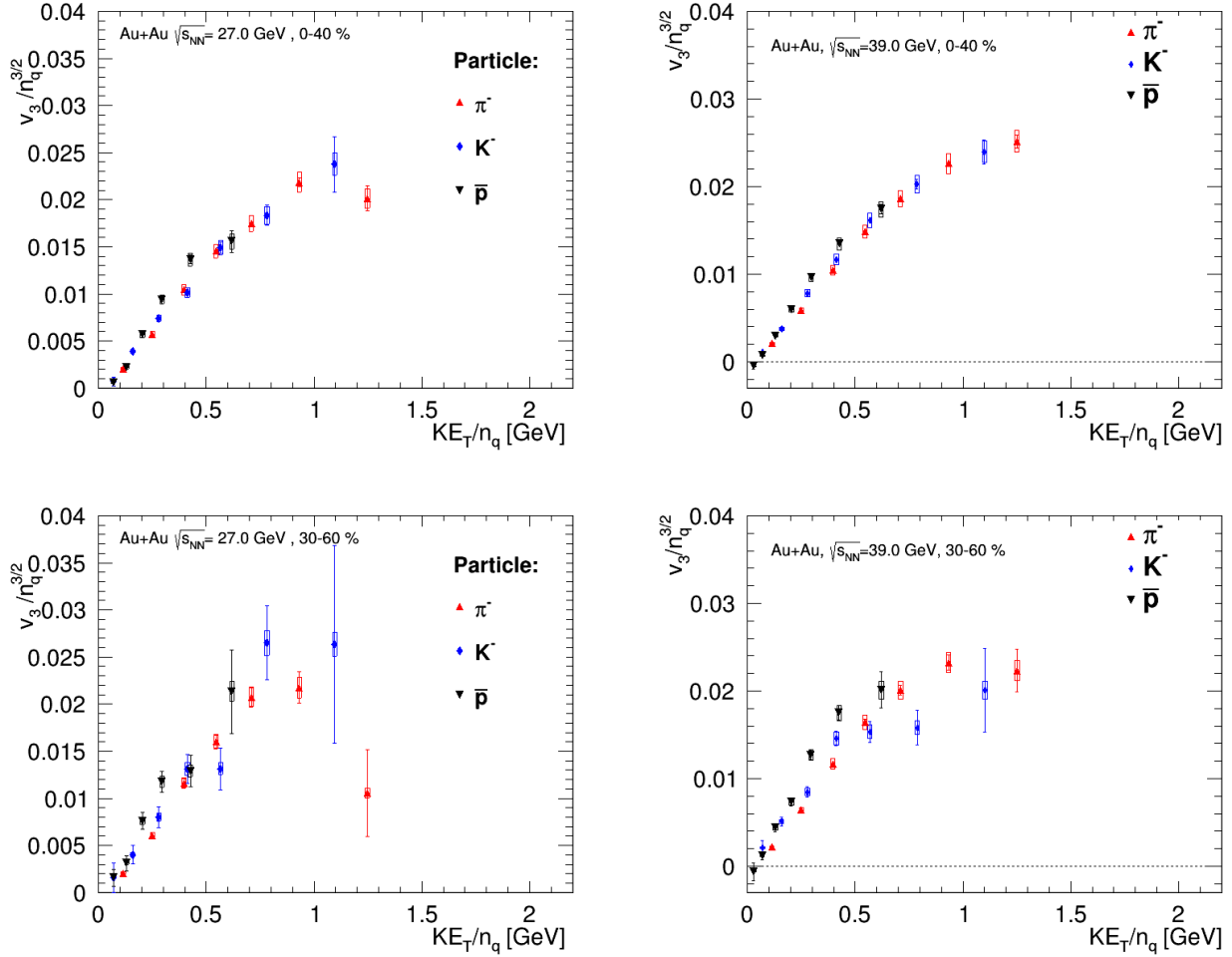


Figure 22: Scaling triangular flow,  $v_3$ , of antiparticle for 0%-40%, 30%-60% centrality Au+Au collisions for energies: on the left - for Au+Au collisions at  $\sqrt{s_{NN}} = 27$ , on the right -  $\sqrt{s_{NN}} = 39$  GeV.

## 5.5 $v_2$ and $v_3$ for particle and antiparticle

The study of particle and antiparticle flow is of a great interest. The results of the STAR [10] collaboration showed that this difference for elliptic flow increases with decreasing energy and is most noticeable for baryons.

Figures 23 and 24 show compare between flow ( $v_2$  and  $v_3$  respectively) of particles and antiparticles for 0%-40% centrality Au+Au collisions at  $\sqrt{s_{NN}} = 27, 39$  GeV. The bottom row of each panel shows the difference between a particle and corresponding antiparticle  $v_2(p_T)$ . It is observed that the flow  $v_2$  and  $v_3$  for positively and negatively charged pions and kaons are consistent for all intervals of centrality. At the same time, the difference between flow for protons and antiprotons is more than 10 %. Figure 25 shows ratio between a particle and corresponding antiparticle  $v_2(p_T)$  and  $v_3(p_T)$  for different energies ( $\sqrt{s_{NN}} = 11.5, 14.5, 19, 27, 39$  GeV).

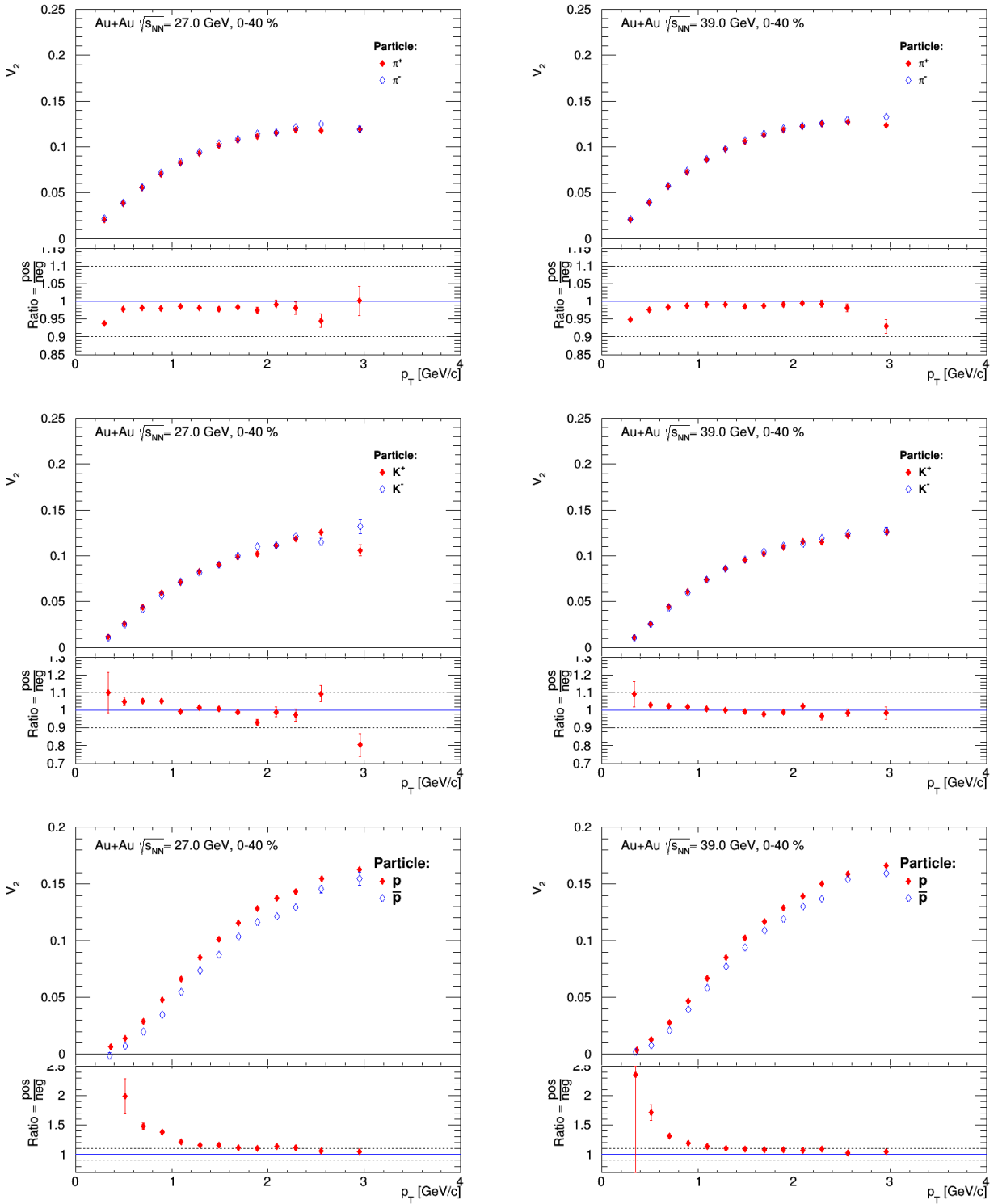


Figure 23: The  $v_2$  as a function of the transverse momentum,  $p_T$ , for 0-40% centrality Au+Au collisions for particle and antiparticle for energies: on the left - for Au+Au collisions at  $\sqrt{s_{NN}}=27$  GeV, on the right -  $\sqrt{s_{NN}}=39$  GeV.

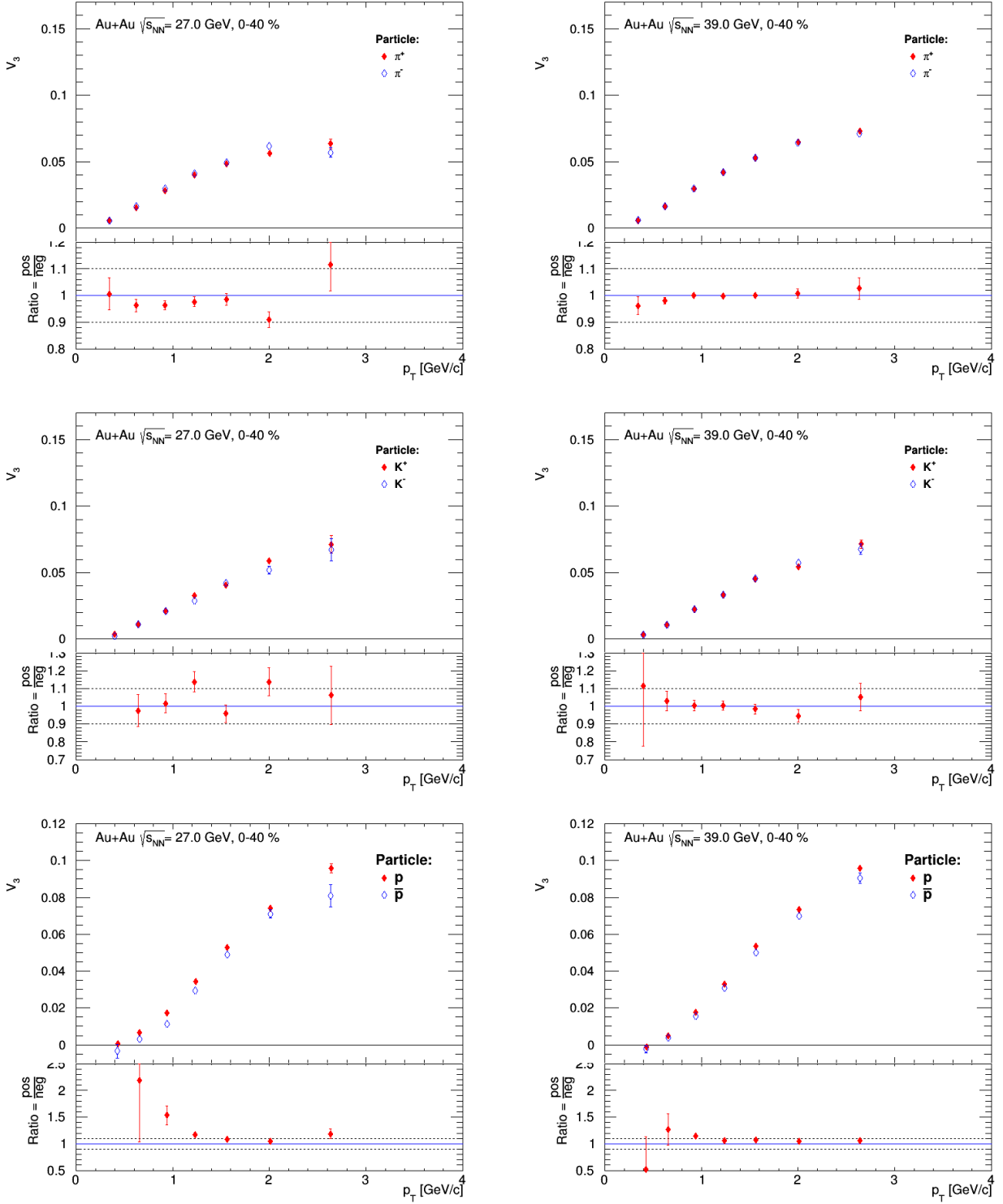


Figure 24: The  $v_3$  as a function of the transverse momentum,  $p_T$ , for 0-40% centrality Au+Au collisions for particle and antiparticle for energies: on the left - for Au+Au collisions at  $\sqrt{s_{NN}}=27$  GeV, on the right -  $\sqrt{s_{NN}}=39$  GeV.

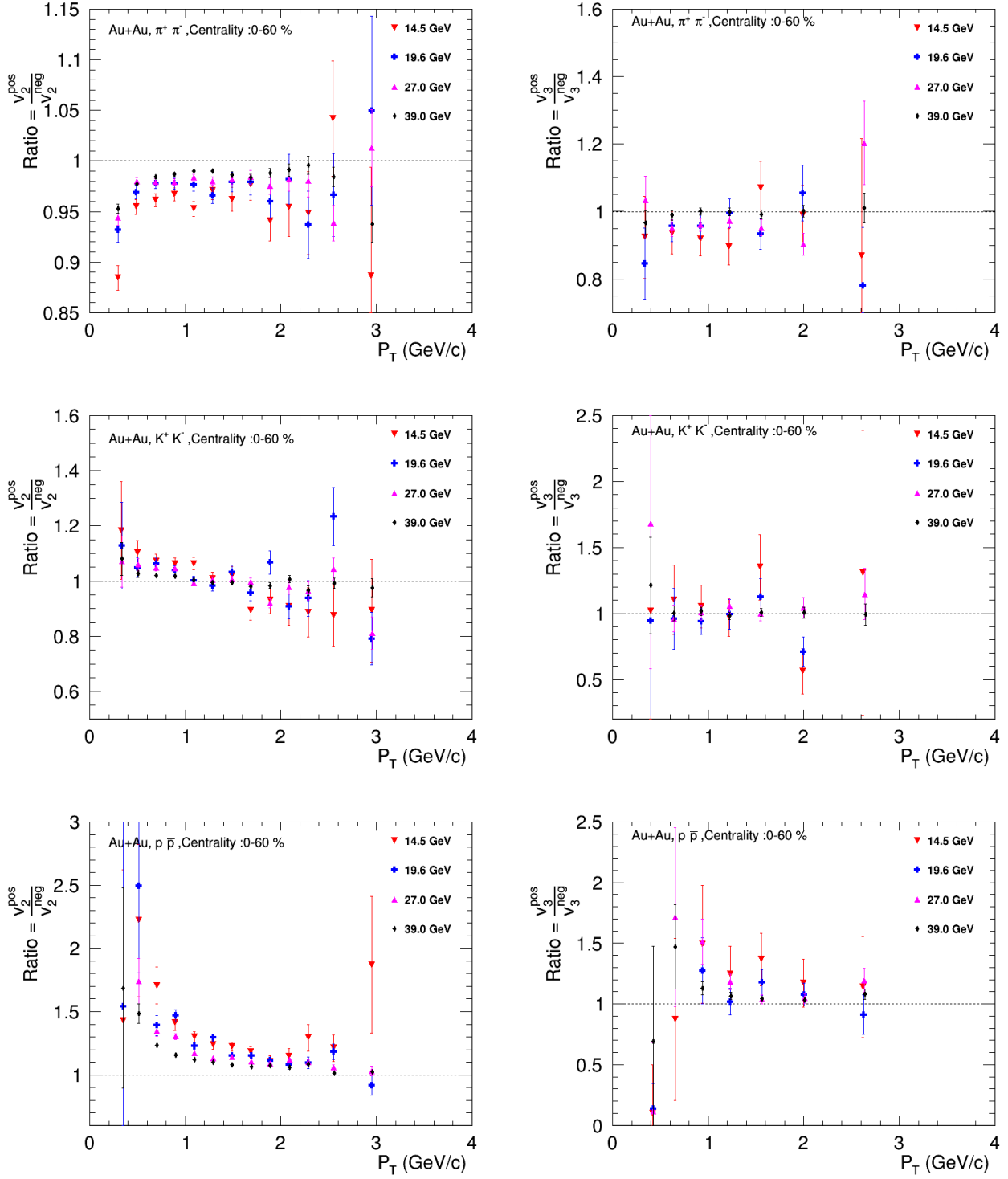


Figure 25: The ratio between a particle and corresponding antiparticle  $v_n(p_T)$  (top  $\pi^+, \pi^-$ , the middle  $K^+, K^-$ , bottom  $p, \bar{p}$ ) for different energies for centrality 0 – 60%: left -  $v_2$ , right -  $v_3$ .

## 6 Conclusion

In this work, we have measured the elliptic  $v_2$  and triangular  $v_3$  flow of charged hadrons and identified particles ( $\pi^\pm, K^\pm, p, \bar{p}$ ).

An analysis of the performances of Au + Au collision data for two energy data sets  $\sqrt{s_{NN}} = 27, 39$  GeV of the STAR experiment was performed. Results on the collective flow measurements of  $v_2$  and  $v_3$  of charged and identified hadrons is presented for the transverse momentum and centrality dependence of the collision. Results for  $v_3$  are new for these energies.

The results of the elliptic flow measurements of charged and identified hadrons were compared with the published data from the STAR collaboration. We can conclude that methods for measuring flows and the method for identifying particles used in the analysis work correctly.

A significant difference in  $v_2(p_T), v_3(p_T)$  between the particles and corresponding antiparticles was observed and observed the ratio it creases with decreasing beam energy. The difference was larger for baryons than for mesons.

## 7 Acknowledgments

I would like to express my gratitude to my supervisor Alexey Aparin for the opportunity and for the support throughout the course of this project. I express my gratitude to Arkadiy Taranenko, my supervisor is Russia, who encouraged me to apply on this program and who advised me throughout my work. Lastly, I would like to thank the Organizing Committee of the Summer Student Program for the amazing opportunity of being part of this experience and for financial support.

# References

- [1] H. Satz Rept. Prog. Phys. 63 (2000) 1511.
- [2] S. A. Bass et al., J. Phys. G 25 (1999) R1.
- [3] A.M.Poskanzer, S.A. Voloshin - "Methods for analyzing anisotropic flow in relativistic nuclear collisions", Phys.Rev.C58 1671-1678, (1998).
- [4] P. Huovinen, and P. V. Ruuskanen. arXiv preprint nucl-th/0605008 (2006).
- [5] Muller, Berndt, and James L. Nagle. arXiv preprint nucl-th/0602029 (2006).
- [6] The RHIC Beam Energy Scan program in STAR, Grazyna Odyniec 2013 J. Phys. Conf. Ser. no. 455 012037
- [7] L. Adamczyk, et al., "Elliptic flow of identified hadrons in Au+Au collisions at  $\sqrt{s_{NN}} = 7.7-62.4$  GeV", Phys. Rev. C88, 014902, (2013).
- [8] L. Adamczyk, et al., "Centrality dependence of identified particle elliptic flow in relativistic heavy ion collisions at  $\sqrt{s_{NN}} = 7.7-62.4$  GeV", Phys. Rev. C93, 014907, (2016).
- [9] D. Molnar, S. Voloshin, Phys.Rev.Lett. 91, 092301, (2003).
- [10] L. Adamczyk et al., (STAR Collaboration) arXiv preprint arXiv:1509.08397.